ARTICLE

DOI: 10.1590/2317-4889201920190010

BJGEO
Brazilian Journal of Geology

Geochemistry, Sm-Nd isotopes and SHRIMP U-Pb geochronology of the Morro do Coco Granite (RJ, Brazil): another piece of the post-collisional magmatism of the Ribeira Belt

Fellippe Roberto Alves Bione[1]*, Everton Marques Bongiolo[1,2], Julio Cezar Mendes[1], Camila Leão Roland[3]

Abstract

The Morro do Coco granite (MC) is a post-collisional intrusive body that was emplaced at Ribeira Belt, in the Cambro-Ordovician, succeeding the final stages of the Gondwana supercontinent amalgamation. This unit requires more studies, contrasting with similar best investigated occurrences of the central Ribeira Belt. This work presents a detailed investigation of such unit using petrography, Inductively Coupled Plasma (ICP), X-Ray Fluorescence (XRF) whole-rock geochemistry, U-Pb (SHRIMP) geochronology and Sm-Nd isotopes. The rock is a nearly undeformed syenogranite, geochemically classified as a high-K calc-alkaline magnesian, with metaluminous to slightly peraluminous affinity. Strongly light rare earth elements (LREE)-enriched patterns with significant negative Eu anomalies, typical of post-collisional granites, are identified. Similarly to other post-collisional granites of the central Ribeira Belt, U-Pb zircon data provide crystallization age of 496 ± 3 Ma . Sm-Nd isotopic data suggest crustal magma source as indicated by $\varepsilon Nd_{(496)}$ of -9, $^{143}Nd/^{144}Nd$ ratios between 0.511747 and 0.511752 and Mesoproterozoic TDM ages of 1.3 Ga. Based on its geochemical characteristics, morphology and geochronology, this unit is considered here as a member of Nova Friburgo Suite. Geochronological data defined three pulses of magmatism in this part of the orogen during the Cambro-Ordovician (515, 490 and 460 Ma).

KEYWORDS: Post-collisional; Brasiliano Orogeny; Cambro-Ordovician; Ribeira Belt; Morro do Coco granite.

INTRODUCTION

During the Neoproterozoic-Paleozoic, Brasiliano/Pan-African thermotectonic events took place at the margins of the São Francisco paleocontinent (Brazil) and another plate located to the east, possibly the Congo paleocontinent (Heilbron *et al.* 2000, Brito Neves *et al.* 2014). The convergence between these two continents and possibly a third one, the Paranapanema block which is presently interpreted as hidden under the Paleozoic Paraná basin in Brazil (*cf.* Trouw *et al.* 2000), resulted in a series of collisions that culminated in the amalgamation of the Gondwana supercontinent from ca. 580 to 510 Ma (*e.g.*, Schmitt *et al.* 2004, Heilbron *et al.* 2008). At Southeastern Brazil, these orogenic events are presently represented by the Ribeira and Araçuaí Belts (Fig. 1A), which extend for more than 1,400 km along Espírito Santo, Rio de Janeiro, São Paulo and Minas Gerais States.

The post-collisional phase, considered here as the ongoing geodynamic stage after the maximum plate convergence and the high-pressure metamorphism of this region, precluded "stable" platform conditions that allowed the development of Paleozoic intracratonic basins such as Amazonas and Paraná (Cunha *et al.* 2007, Milani *et al.* 2007). Indeed, the post-collisional stage is considered a complex period of large horizontal terrane adjustments along shear zones, associated to crustal extension and uplift, lithospheric delamination, docking and subduction of oceanic plates (*e.g.*, Liégeois 1998). The post-collisional magmatism at Ribeira and Araçuaí Belts encompasses mainly high-K calc-alkaline granitoids, minor dioritic and a single manifestation of true shoshonitic rocks (*e.g.*, Martins *et al.* 2016).

In this paper, the first study of the Morro do Coco granite (MC) is provided by presenting its field, petrographic and geochemical features, U-Pb zircon geochronology and Sm-Nd isotopic data in order to contribute to the understanding of the post-collisional magmatism that took place in Southeast Brazil during the Cambro-Ordovician period. Previous data of similar occurrences in the same region were also compared and discussed regarding the geographic and age distribution of intrusions with similar age to reconstruct the regional geodynamic scenario during the post-collisional stage of the Gondwana supercontinent amalgamation.

Supplementary material

Supplementary data associated with this article can be found in the online version: Supplementary Table A1, Supplementary Table A2, Supplementary Table A3, Supplementary Table A4 and Supplementary Table A5.

[1]Programa de Pós-graduação em Geologia, Instituto de Geociências, Universidade Federal do Rio de Janeiro – Rio de Janeiro (RJ), Brazil. E-mails: frbione.geo@gmail.com, embongiolo@hotmail.com, julio@geologia.ufrj.br

[2]Instituto de Geociências, Universidade Federal do Rio Grande do Sul – Porto Alegre (RS), Brazil.

[3]Programa de Pós-graduação em Geoquímica, Instituto de Química, Universidade Federal Fluminense – Niterói (RJ), Brazil. E-mail: camila.leaoroland@gmail.com

*Corresponding author.

GEOLOGICAL SETTING

The Ribeira Belt (Fig. 1B) is commonly divided into four tectonostratigraphic domains, with rocks verging northwest toward the São Francisco Craton (SFC; *e.g.*, Trouw *et al.* 2000) namely, from bottom to top:

- Occidental Terrane, the autochthonous domain, composed by intercalations of reworked SFC sheets interleaved with Meso-Neoproterozoic metasedimentary rocks from its passive margin;
- the Embú-Paraíba do Sul Terrane, considered a magmatic arc resulting from the subduction and collision between the São Francisco and the Paranapanema paleocontinents (Trouw *et al.* 2013). It consists of Paleoproterozoic orthogneiss and metasedimentary rocks, and Neoproterozoic granitoids intrusive in the orthogneisses;
- the Oriental Terrane, comprising paragnaisses intruded by syn-collisional granitoids (Costeiro Domain), Rio Negro Magmatic Arc (ca. 780 to 620 Ma; Tupinambá *et al.* 2000) and post-collisional granitoid intrusions (ca. 515–454 Ma; Valeriano *et al.* 2011, Tupinambá *et al.* 2012, Bongiolo *et al.* 2016), including MC, focus of this contribution;
- The Cabo Frio Tectonic Domain (CFTD), considered as part of the Congo Craton (*e.g.*, Fernandes *et al.* 2015). The CFTD constitutes a Paleoproterozoic basement (Região dos Lagos Complex; Fonseca *et al.* 1979), represented by calc-alkaline orthogneisses of tonalitic to syenogranitic compositions, tectonically interleaved with Neoproterozoic metavolcano-sedimentary successions (Búzios and Palmital; Schmitt *et al.* 2004).

The main periods of thermotectonic activity recorded at the Ribeira Belt are:

- ca. 790–620 Ma, pre-collisional stage, including subduction and development of magmatic arcs such as Rio Negro and Serra da Bolívia (Tupinambá *et al.* 2012; Heilbron *et al.* 2013);
- 620–605 Ma, collisional stage between the Embú-Paraíba do Sul microcontinent and the São Francisco Craton passive margin (Trouw *et al.* 2013) that originated the southern Brasilia Belt;
- 605–550 Ma, collisional stage between a continental arc and the Oriental Terrane, representing the main collisional event registered at the Ribeira Belt (Heilbron and Machado 2003);
- 540–510 Ma, the docking of the Cabo Frio Terrane against the Oriental Terrane in the Buzios Orogeny (Schmitt *et al.* 2004);
- 510–440 Ma, when post-collisional magmatism took place in the Oriental Terrane (Valeriano *et al.* 2016, Schmitt *et al.* 2004, Bongiolo *et al.* 2016).

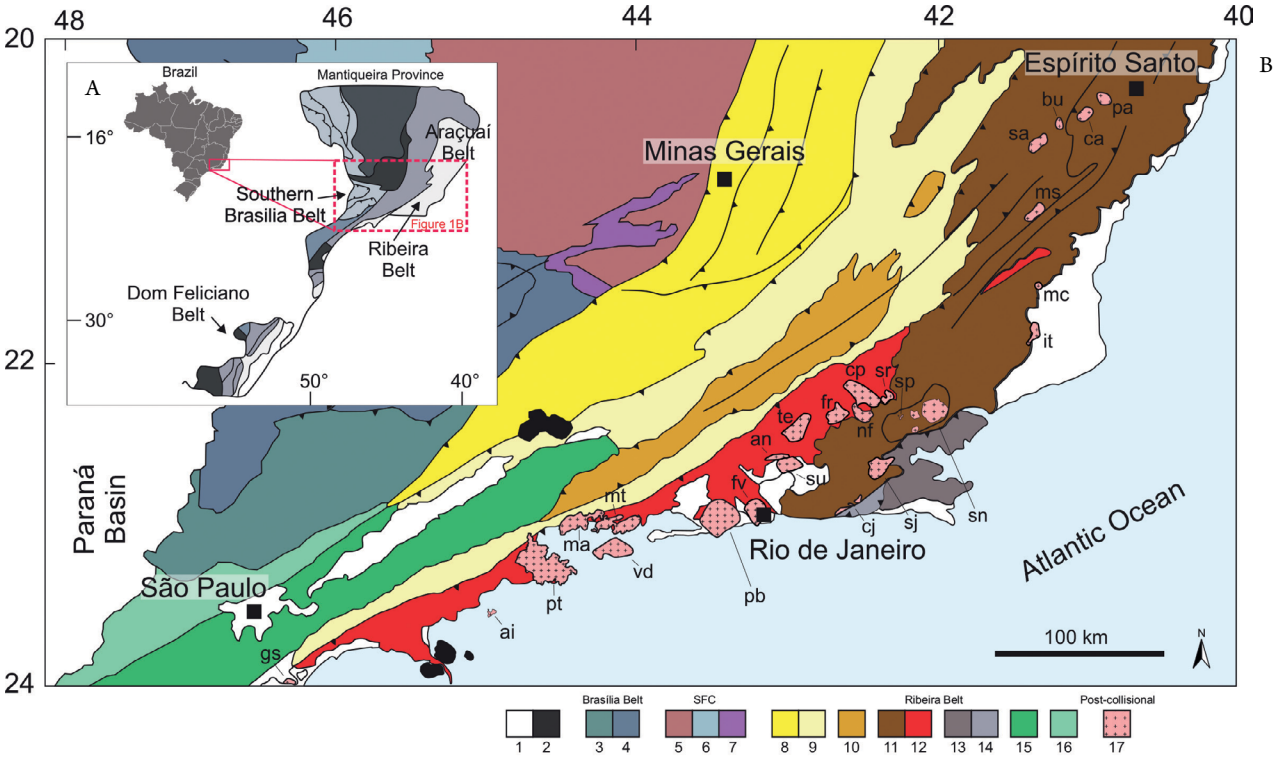

Figure 1. Regional maps and tectonic context (modified from Heilbron *et al.* 2004). (A) Subdivision of the Mantiqueira Province, composed by the Brasilia, Dom Feliciano, Ribeira and Araçuaí Belts and location of Figure 1B area (dashed square). (B) Tectonic map of the Central segment of the Mantiqueira Province: (1) Cenozoic rifts covers; (2) Cretaceous alkaline massifs; (3) Socorro-Guaxupé Nappe (superior nappe); (4) Metasedimentary rocks including Ky-granulites (Inferior nappes); (5) São Francisco Craton basement and autochthonous domain; (6) São Francisco Supergroup; (7) São João Del Rey and Tiradentes formations (autochthonous covers); (8) Andrelandia Group; (9) Juiz de Fora domain (Occidental Terrane); (10) Paraíba do Sul Klippe; (11) Oriental Terrane Gneiss complex; (12) Rio Negro magmatic arc granitoids; (13) Cabo Frio Tectonic Domain Região dos Lagos Ortogneiss; (14) Cabo Frio Tectonic Domain Búzios-Palmital supracrustal sucessions; (15) Embu terrane; (16) São Roque and Açungui terranes; (17) Cambro-Ordivician granitoids: gs- Guarujá-Santos; ai- Anchieta Island; pt- Parati; ma- Mambucaba; mt- Mangaratiba; vd- Vila dois Rios; pb- Pedra Branca; fv- Favela; an- Andorinha; su- Suruí; te- Teresópolis; fr- Frade; nf- Nova Friburgo; cp- Conselheiro Paulino; sr- São José do Ribeirão; sp- São Pedro de Lumiar; sn- Sana; sj- Silva Jardim; cj- Cajú; it- Itaoca; mc- Morro do Coco; ms- Mimoso do sul; sa- Santa Angélica; bu- Buarama; ca- Castelo; pa- Pedra Azul.

This complete history of subductions and orogenies recorded at Ribeira Belt resembles a long-term maintenance of high temperatures and low cooling rates at the active (upper) plate. Thus, Ribeira Belt is considered a hot orogen (*e.g.*, Bento dos Santos *et al.* 2010, 2015, Valeriano *et al.* 2016), which might have implications on the post-collisional magmatism observed throughout its entire area.

The Cambro-Ordovician magmatism at the Ribeira-Araçuaí belts

Several occurrences of post-collisional Cambro-Ordovician granitoids, and fewer records of intermediate and basic rocks (De Campos *et al.* 2004, Valeriano *et al.* 2017) are found at the Ribeira and Araçuaí belts (Fig. 1B). Valeriano *et al.* (2011, 2016) summarize the occurrence and characteristics of the 15 largest granitic intrusions in the Central Ribeira Belt. Based on geochronological, compositional and structural characteristics, Valeriano *et al.* (2011, 2017) individualized two groups of post-collisional intrusions:

- the Cambrian Suruí Suite (ca. 510 Ma);
- the Ordovician Nova Friburgo Suite (ca. 485 Ma).

At the Central Ribeira Belt, other smaller post-collisional bodies are known, such as the Cajú granite (454 ± 5 Ma; Bongiolo *et al.* 2016); the São Pedro de Lumiar granite (~490 Ma; Mendes *et al.* 2011); the Mambucaba granite (492 ± 15; Machado *et al.* 1996) and the MC granite, focus of this study.

Cambro-Ordovician intrusions also occur at the northern area where there is a transition between the Ribeira and the Araçuaí belts, like the Santa Angélica (513 ± 8 Ma; Söllner *et al.* 2000), Mimoso do Sul and Buarama (495 ± 5 Ma and 480 ± 4 Ma, respectively; Söllner *et al.* 2000) and Várzea Alegre (499 ± 5 Ma; Mendes *et al.* 2005) bimodal intrusive bodies. Post-collisional granitic intrusions have also been identified at the southern Ribeira Belt, such as the Guarujá-Santos granites (497 ± 7 Ma; Janasi *et al.* 2015) and the Anchieta Island (500 ± 6 Ma; Azevedo Sobrinho *et al.* 2011).

The geographic distribution of these intrusions along a NE/SW relatively restricted corridor of about 80 km width inside the Oriental Terrane (Fig. 1B) raises ideas about the geodynamic models responsible for their emplacement, which Valeriano *et al.* (2016) suggest to be a response to break-off of the subducted lithospheric slab and production of localized post-collisional magmatism along a narrow zone in the upper plate.

ANALYTICAL METHODS

Sampling and petrography

Geological mapping and sampling were carried out at the MC region (Fig. 2). The granite and its host rocks were sampled prioritizing fresh rocks and scattering in the mapped area. Eight thin sections of MC granite were studied under transmitted light petrography at the Universidade Federal do Rio de Janeiro (UFRJ). Modal mineral distribution was obtained for all samples by counting at least 600 points per thin section. The plagioclase composition was petrographically calculated using the a-normal extinction-angle method (*cf.* Hibbard 1995).

Lithogeochemistry

Nine whole-rock samples from MC granite (Suppl. Tab. 1A) were analyzed by Inductively Coupled Plasma Atomic Emission Spectrometry (ICP-AES) to evaluate major elements plus MnO, BaO, Cr_2O_3 and SrO, and by ICP Mass Spectrometry (ICP-MS) to determine trace elements at the ALS laboratory, Canada. Samples were digested by Lithium tetraborate fusion prior to nitric acid dissolution, before analyses. Duplicate and blank samples were used to control the analyses' accuracy and precision, respectively. Loss on Ignition (LOI) was obtained by heating the samples at 1,000ºC for over an hour. Five other

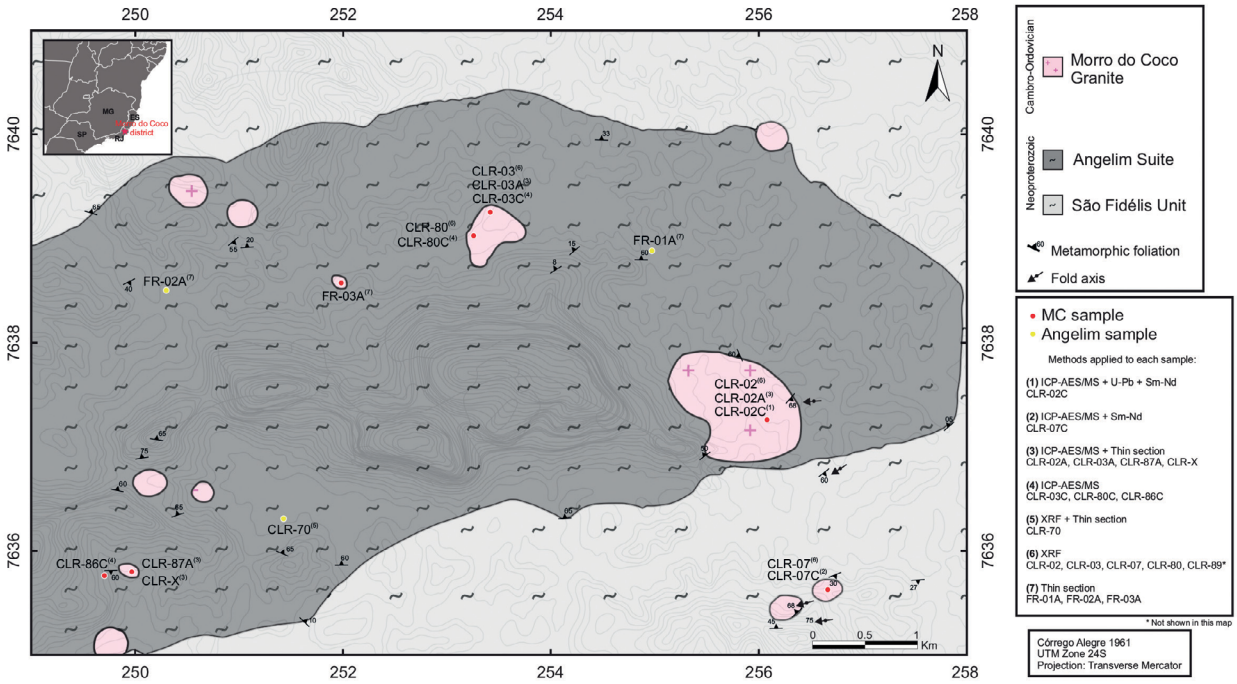

Figure 2. Geological Map of the Morro do Coco Granite and geographic location of the samples used in this work.

samples were analyzed by X-Ray Fluorescence (XRF) (Philips PW2400 with Rh-bearing tube) for major and some trace elements in the XRF laboratory at UFRJ. Duplicate analyses showed comparable results between the laboratories. All results were recalculated to anhydrous totals after Fe-oxidation adjustment to obtain the Fe_2O_3/FeO ratios from the $Fe_2O_{3(t)}$ measured (*cf.* Middlemost 1989) using the IgRoCS software (Verma and Rivera-Gómez 2013). Adjusted data were used to calculate CIPW norms and were plotted on multidimensional tectonic discrimination diagrams for acidic rocks using the TecDIA software of Verma *et al.* (2015). Other chemical classification, geotectonic discriminant and elemental diagrams developed by several authors were plotted using the GeoChemical Data toolkit 5.0 (GCDkit; Janoušek *et al.* 2006).

Zircon U-Pb geochronology

In-situ high resolution SHRIMP dating on zircon crystals was performed on one sample (CLR-02C) from MC granite. Zircon crystals were concentrated by magnetic and heavy liquid separation prior to handpicking under binocular microscope. The sample was mounted on adhesive tape, placed on epoxy resin, and polished. TEMORA 1 zircon ($^{206}Pb/^{238}U$ age of 416.78 ± 0.33 Ma; Black *et al.* 2003) was used as standard. Zircon grains were assessed under cathodoluminescence (CL) imaging to determine its internal domains and to select the spots for analysis. Isotopic data was acquired by a SHRIMP IIe at the Geochronology Research Center (CPGeo; Universidade de São Paulo). Softwares used at the CPGeo were LabVIEW 8.5 and SHRIMP SW 2.1. Raw data reduction was done using SQUID 1.06 Excel macro (Ludwig 2001), and concordia diagrams were plotted using ISOPLOT 4.15 (Ludwig 2012). U concentration was calibrated against the standard crystal SL13 with 238 ppm of U (Claué-Long *et al.* 1995, Sato *et al.* 2014). Common lead corrections were made to ^{204}Pb (*cf.* Stacey and Kramers 1975). The uncertainties of isotopic ratios and ages were reported at the 1% level, and weighted mean ages were reported as 95% confidence limits (Sato *et al.* 2014).

Whole-rock Sm-Nd isotopes

Whole-rock Sm-Nd isotope analyses on two samples (CLR-02C and CLR-07C) were carried out by ICP-MS (Thermo Neptune) at CPGeo, following the procedures described by Sato *et al.* (1995). Prior to ICP-MS analysis, Sm and Nd concentrations were obtained through isotope dilution, with the addition of a ^{149}Sm and ^{150}Nd combined spike, followed by chemical digestion by HF, HNO_3 and HCl in Savillex™ vessels. Chromatographic separation of Sm and Nd was achieved in two steps, starting with AG50W-X8 resin to separate Rare Earth Elements (REE) from the bulk sample, followed by Sm and Nd separation using LaNthanides (LN) resin. Isotopic $^{143}Nd/^{144}Nd$ ratios were normalized to $^{146}Nd/^{144}Nd = 0.7219$ (DePaolo 1981). $^{147}Nd/^{144}Nd$ ratios and $eNd_{(t)}$ values were calculated according to Hamilton *et al.* (1983). Analytical blank concentration was 31pg and the mean value for $^{143}Nd/^{144}Nd$ of JNDi standard from July to May 2014 was 0.512097 ± 0.000005. Resulting data was plotted using ISOPLOT 4.15 (Ludwig 2012).

FIELD ASPECTS AND PETROGRAPHY

MC granite is a tabular plutonic body that occupies an area of about 45 km^2 at northern Rio de Janeiro State, Brazil (Fig. 2). It is intrusive in paragneiss of the São Fidélis Unit and ortogneiss of the Angelim Suite, both part of the Neoproterozoic Costeiro Domain of the Central Ribeira Belt (Fig. 1B). São Fidélis Unit comprises a supracrustal sequence of the Costeiro Domain, consisted of paragneiss metamorphosed under amphibolite facies P-T conditions (Eirado *et al.* 2017). In the studied area, it occurs as garnet-biotite-sillimanite gneiss, cropping out at lower topographic areas. The Angelim Suite ortogneiss is a group of intrusive plutonic rocks of predominant tonalitic composition in the supracrustal São Fidélis Unit (Tupinambá *et al.* 2007). It is represented in the studied area by a garnet-hornblende-biotite gneiss, cropping out at higher topographies.

In the field, MC occurs mostly as *in situ* blocks and boulders. The rock is macroscopically very homogeneous throughout the studied area. Its modal proportions plot in the field of syenogranites in the Quartz, Alkali feldspar, Plagioclase (QAP) diagram (Suppl. Tab. A2 and A3).

Petrographically, MC is a grey, leucocratic, equigranular, medium-grained (3 mm in average) rock composed essentially by quartz (27%), alkali-feldspar (28%), biotite (16%) and plagioclase (10.5%). Allanite, titanite, apatite, opaque minerals and rare rutile are the accessory phases. Chlorite and sericite are the main secondary minerals (Fig. 3). Quartz occurs as subhedral to anhedral crystals, varying from 0.5 to 3 mm, and locally show undulose extinction (Figs. 3G and 3H); alkali-feldspar occurs as subhedral to euhedral crystals varying between 0.5 to 4.5 mm, often showing Carlsbad and tartan twinning and alteration to sericite; recrystallization of alkali-feldspar subcrystals is also observed locally (Figs. 3K and 3L).

Biotite is light to dark brown, subhedral to euhedral varying from 0.1 to 1 mm and usually occurs as inclusions in quartz. Alteration to chlorite and opaque minerals is observed. Plagioclase crystals are anhedral to subhedral, with grain size ranging from 0.2 to 2 mm, and generally show polysynthetic twinning. Myrmekitic texture is locally observed in plagioclase crystals rimmed by alkali-feldspar (Figs. 3I and 3J). Alteration to sericite can be observed on plagioclase, whose measured plagioclase composition is compatible with andesine (An_{34-38}).

Titanite occurs as light brown, subhedral to anhedral crystals of 0.5 mm on average. They may present alteration to opaque minerals within crystal borders and fractures. Epidote occurs as prismatic, with yellow color and pleochroism, subhedric to euhedric, 0.5 to 1 mm crystals with allanite cores (Figs. 3E and 3F). Zircon crystals are subhedral to anhedral, measuring up to 0.3 mm and occur mostly included within quartz and biotite crystals (Figs. 3C and 3D) and apatite occurs as submillimetric rounded crystals.

RESULTS

Whole rock geochemistry

Whole-rock major and trace elements analyses were performed on 14 MC granite samples (Tab. 1). SiO_2 content

varies from 68 to 72 wt.%, Al_2O_3 concentrations are between 14 and 15 wt.%, K_2O has high concentrations of up to 6 wt.%, and CaO and Na_2O have average contents of 2 to 2.8 wt.%, respectively. Average $Fe_2O_{3(t)}$ content is 2.9 wt.%.

MC granites are characterized by high Ba (~1,700 ppm), Zr (~500 ppm), Th (~75 ppm) and light rare earth elements (LREE) (La 225 ppm and Ce ~435 ppm), and medium Sr contents (~340 ppm). Nonetheless, heavy rare earth elements (HREE) show small concentrations such as Yb (0.7 ppm) and Lu (0.1 ppm).

The CIPW normative mineralogy (Suppl. Tab. A4) corresponds to quartz (ca. 23-29 wt.%), orthoclase (ca. 33-37 wt.%), plagioclase (ca. 28-36 wt.%), and lesser amounts of hypersthene, magnetite, ilmenite, apatite and normative corundum, which is compatible with petrographic results.

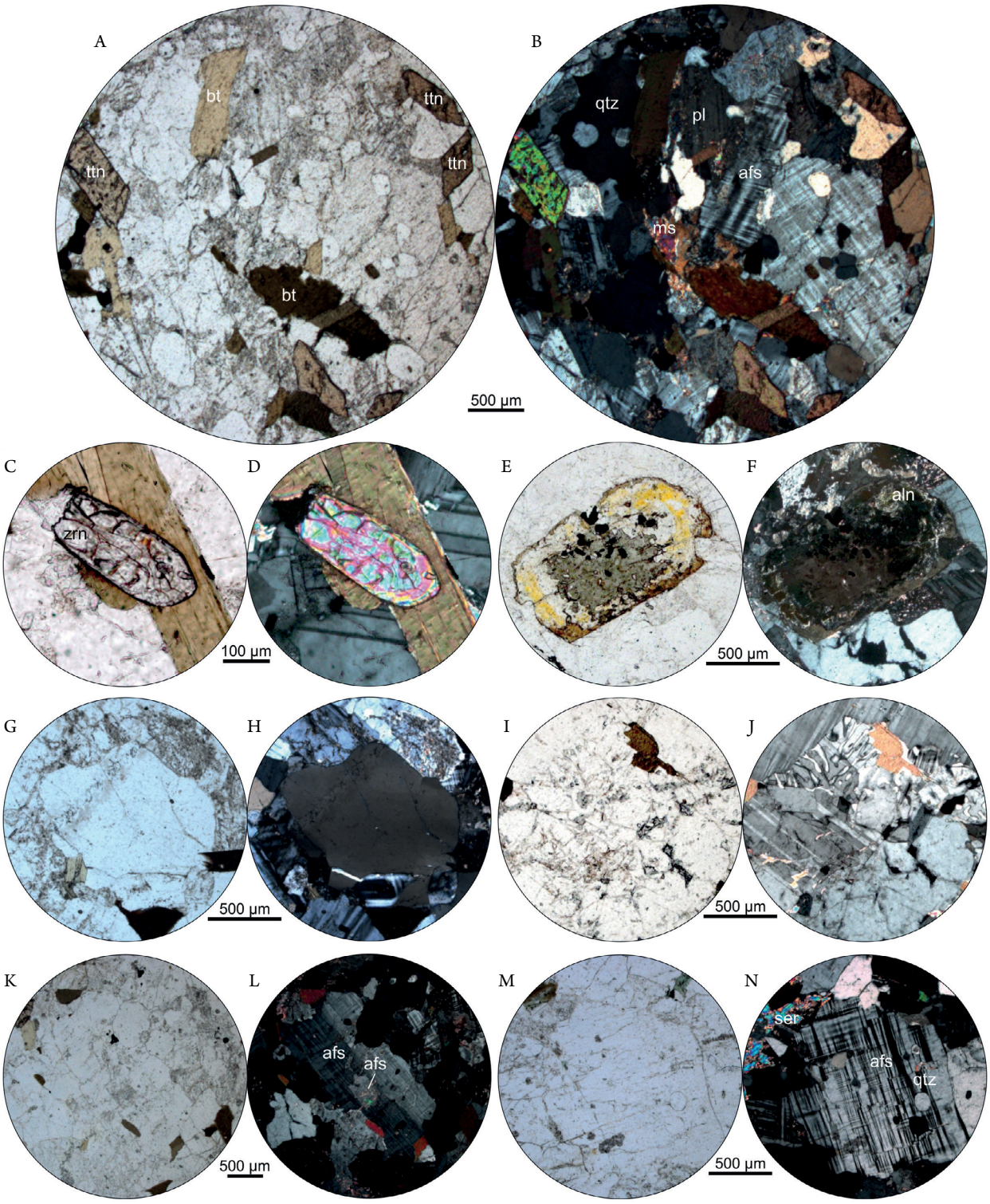

qtz: quartz; afs: alkali-feldspar; bt: biotite; pl: plagioclase; ttn: titanite; aln: allanite; zrn: zircon; chl: clorite; ser: sericite.

Figure 3. Photomicrographs of Morro do Coco. Each pair of photomicrographs is shown as parallel and crossed polars, respectively. (A) and (B) General aspects of mineralogy and texture of the granite; (C) and (D) Zircon crystal on detail; (E) and (F) Yellow epitode crystal with allanite core; (G) and (H) Detail on quartz crystal showing undulose extinction; (I) and (J) Detail on plagioclase crystal and myrmekitic texture on plagioclase near alkali-feldspar; (K) and (L) Detail on alkali-feldspar subcrystal in larger alkali-feldspar crystal; (M) and (N) Detail on quartz crystal in alkali-feldspar.

The studied granites are high-K calc-alkaline, magnesian to ferroan and metaluminous to slightly peraluminous (Fig. 4). In the K_2O *vs.* SiO_2 diagram (Fig. 4B), MC samples plot in the shoshonite series field. However, they are considered here as high-K calc-alkaline rocks, as they do not meet all the requirements to be classified as a true shoshonite (*cf.* Morrison 1980, Campbell *et al.* 2014), such as:

- $Na_2O/K_2O > 1$ at 55 wt% SiO_2;
- negative or absent correlation between K_2O *vs.* SiO_2 at $SiO_2 > 57$ wt%;
- La/Yb_N between 8 and 46.

Using multielemental diagram normalized to the average crust (Weaver and Tarney 1984; Fig. 5A), MC samples display moderate enrichment in large ion litophile elements (LILE) such as Rb, Th and K and are less enriched in high field strength elements (HFSE) such as P and Ti. Negative Sr, Ba, P, Nb, Ti and Zr anomalies would indicate fractionation of plagioclase, apatite, titanite and zircon. The chondrite-normalized REE

Table 1. Representative geochemical analyses of Morro do Coco granite by Inductively Coupled Plasma Atomic Emission Spectrometry (ICP-AES) (major elements), Inductively Coupled Plasma Mass Spectrometry (ICP-MS) (trace elements) and X-Ray Fluorescence (XRF) (major and trace elements).

	Combined ICP-AES and ICP-MS									XRF				
	CLR-02A	**CLR-02C**	**CLR-03A**	**CLR-03C**	**CLR-07C**	**CLR-80C**	**CLR-86C**	**CLR-87A**	**CLR-X**	**CLR-02**	**CLR-03**	**CLR-07**	**CLR-80**	**CLR-89**
SiO_2	68.30	69.00	68.70	68.50	68.40	70.10	71.10	71.00	72.00	67.96	67.87	70.52	68.32	70.32
TiO_2	0.77	0.75	0.80	0.76	0.95	0.72	0.47	0.42	0.42	0.80	0.75	0.44	0.71	0.44
Al_2O_3	14.55	14.85	14.80	14.65	14.50	14.50	13.95	13.80	13.95	15.25	15.39	14.42	15.13	14.82
Fe_2O_3	2.98	2.95	3.03	2.98	3.61	2.78	2.84	2.66	2.71	3.14	3.03	2.78	2.66	2.65
MnO	0.02	0.02	0.03	0.02	0.04	0.03	0.03	0.03	0.03	0.02	0.02	0.03	0.03	0.03
MgO	0.93	0.95	0.93	0.91	1.02	0.83	0.58	0.51	0.51	0.97	0.94	0.55	0.82	0.53
CaO	2.16	2.17	2.22	2.17	2.19	2.11	1.80	1.66	1.69	2.08	2.03	1.55	1.98	1.79
K_2O	5.51	5.80	5.87	5.56	5.56	5.67	5.95	5.95	6.05	5.72	5.81	6.20	5.94	5.99
Na_2O	3.03	3.06	2.95	3.09	2.77	2.98	2.51	2.44	2.49	3.17	3.22	2.45	3.07	2.78
P_2O_5	0.20	0.19	0.22	0.20	0.26	0.17	0.11	0.10	0.11	0.19	0.18	0.09	0.15	0.09
SrO	0.06	0.06	0.05	0.05	0.04	0.03	0.02	0.02	0.02	-	-	-	-	-
BaO	0.25	0.26	0.26	0.24	0.22	0.18	0.13	0.12	0.12	-	-	-	-	-
L.O.I	0.96	0.83	0.77	0.87	0.89	0.93	0.87	0.83	0.84	0.71	0.79	0.91	0.74	0.67
Total	99.72	100.89	100.63	100.00	100.45	101.03	100.36	99.54	100.94	100.01	100.03	99.94	99.55	100.11
ASI*	0.98	0.97	0.97	0.97	1.00	0.97	1.01	1.02	1.02	1.00	1.01	1.06	1.00	1.04
K*	0.54	0.55	0.57	0.54	0.57	0.56	0.61	0.62	0.62	0.54	0.54	0.62	0.56	0.59
CaO/Na_2O	0.71	0.71	0.75	0.70	0.79	0.71	0.72	0.68	0.68	0.66	0.63	0.63	0.64	0.64
Rb	205.00	206.00	245.00	203.00	238.00	230.00	246.00	242.00	255.00	76.00	74.00	187.00	171.00	182.00
Ba	2180.00	2270.00	2300.00	2130.00	1925.00	1555.00	1140.00	1005.00	1070.00	1933.00	1873.00	1196.00	1518.00	1195.00
Sr	506.00	512.00	487.00	486.00	386.00	327.00	207.00	186.00	197.50	426.00	389.00	62.00	275.00	168.00
Th	68.00	57.00	60.20	77.60	60.20	75.80	99.50	107.50	114.00	-	-	-	-	-
U	1.92	1.90	2.04	2.08	3.37	2.44	2.01	2.56	2.72	-	-	-	-	-
Zr	646.00	617.00	684.00	632.00	823.00	622.00	435.00	375.00	402.00	407.00	382.00	275.00	340.00	286.00
Ga	25.60	25.20	25.70	25.80	27.40	26.20	22.60	22.30	23.50	5.00	7.00	5.00	6.00	6.00
Nb	10.10	9.60	11.50	10.90	16.40	11.60	17.70	16.70	19.10	17.00	17.00	13.00	16.00	14.00
Ni	-	-	-	-	-	-	-	-	-	35.00	33.00	34.00	35.00	33.00
Co	-	-	-	-	-	-	-	-	-	9.00	10.00	11.00	11.00	11.00
Zn	-	-	-	-	-	-	-	-	-	28.00	24.00	28.00	31.00	24.00
V	46.00	46.00	48.00	46.00	49.00	39.00	24.00	20.00	23.00	69.00	69.00	51.00	68.00	51.00
Cr	20.00	10.00	20.00	10.00	10.00	20.00	< 10	20.00	20.00	12.00	38.00	3.00	35.00	23.00
Sn	2.00	3.00	3.00	3.00	4.00	2.00	2.00	2.00	3.00	-	-	-	-	-
La	229.00	199.50	234.00	272.00	201.00	205.00	232.00	229.00	241.00	-	-	-	-	-
Ce	434.00	381.00	439.00	511.00	396.00	403.00	460.00	453.00	478.00					
Pr	42.90	38.20	43.90	50.80	42.30	40.80	47.20	47.20	49.80	-	-	-	-	-
Nd	133.00	122.00	136.50	159.50	141.50	131.00	151.00	150.50	159.00	-	-	-	-	-
Sm	14.35	14.25	15.15	18.00	17.05	15.00	19.35	19.45	20.60	-	-	-	-	-
Eu	2.01	1.98	2.12	2.19	2.33	1.63	1.70	1.60	1.74	-	-	-	-	-
Gd	6.13	5.90	6.67	7.34	7.50	6.22	9.42	9.54	10.15	-	-	-	-	
Tb	0.61	0.59	0.66	0.76	0.84	0.68	1.00	1.01	1.06	-	-	-	-	-
Dy	2.35	2.35	2.71	3.04	3.55	2.66	4.15	3.77	3.97	-	-	-	-	-
Ho	0.37	0.34	0.42	0.46	0.56	0.43	0.59	0.55	0.57	-	-	-	-	-
Er	0.84	0.83	0.97	0.96	1.27	0.90	1.32	1.09	1.19	-	-	-	-	-
Tm	0.10	0.09	0.10	0.13	0.17	0.11	0.15	0.13	0.15	-	-	-	-	-
Yb	0.57	0.43	0.67	0.61	0.94	0.59	0.82	0.75	0.79	-	-	-	-	-
Lu	0.07	0.07	0.09	0.07	0.12	0.09	0.11	0.11	0.11	-	-	-	-	-
Y	9.10	9.30	10.60	10.90	15.00	10.30	15.20	13.50	14.50	14.00	14.00	16.00	14.00	15.00
Cs	1.26	0.87	1.50	0.90	1.36	0.85	0.83	1.20	1.23	-	-	-	-	-
Ta	0.70	0.80	0.90	0.80	1.10	1.00	1.00	0.70	1.80	-	-	-	-	-
Hf	15.60	14.20	15.60	15.00	19.30	15.40	12.10	10.90	11.20	-	-	-	-	-
Rb/Sr	0.41	0.40	0.50	0.42	0.62	0.70	1.19	1.30	1.29	-	-	-	-	-
Ba/Rb	10.63	11.02	9.39	10.49	8.09	6.76	4.63	4.15	4.20	-	-	-	-	-
$La/Yb_{(N)}$	270.86	312.79	235.46	300.62	144.16	234.25	190.75	205.85	205.67	-	-	-	-	

Major (wt.%) and selected trace element (ppm); ASI* = $Al_2O_3/CaO + Na_2O+K_2O$ molar ratio; K*= K/Na + K molar ratio.

pattern of Boynton (1984; Fig. 5B) is strongly fractionated, with $(Ce/Yb)_N$ ratios ranging from 109 to 229 and significant negative Eu anomalies ($Eu/Eu^* = 0.37$ to 0.66).

In binary diagrams using silica as differentiation index, major elements present negative correlation for Al_2O_3, CaO, MgO, Na_2O, TiO_2, P_2O_5 and $Fe_2O_{3(t)}$. Positive correlations only occur for K_2O and K_2O/Na_2O (Fig. 6). Minor and trace elements (Fig. 7), exhibit negative SiO_2 correlation for Sr, Zr and Ba and positive correlations for Y and Nb. Other elements such as La show random distribution. Nb/Zr *vs.* Nb binary diagram, used to identify crystal fractionation and different magma sources (Sial and McReath 1984), shows two different clusters for MC samples (Fig. 8) and two evolution lines of fractional crystallization.

Geotectonic classification

A series of geotectonic classification diagrams for acidic rocks were created by Verma *et al.* (2012, 2013) based on linear discriminant analysis of natural logarithm transformed ratios of major (*m3*) and immobile trace elements (*tacid*). The plot of MC in these function-based multidimensional diagrams indicates the rock has collisional affinity on the major elements-based diagrams (m3; Fig. 9), and collisional affinity trending to arc setting on the immobile trace elements-based diagrams (*tacid*; Fig. 10).

In addition, this classification provides a helpful statistical evaluation of the probability the rock has to belong to a specific geotectonic setting (Tab. 2). For the

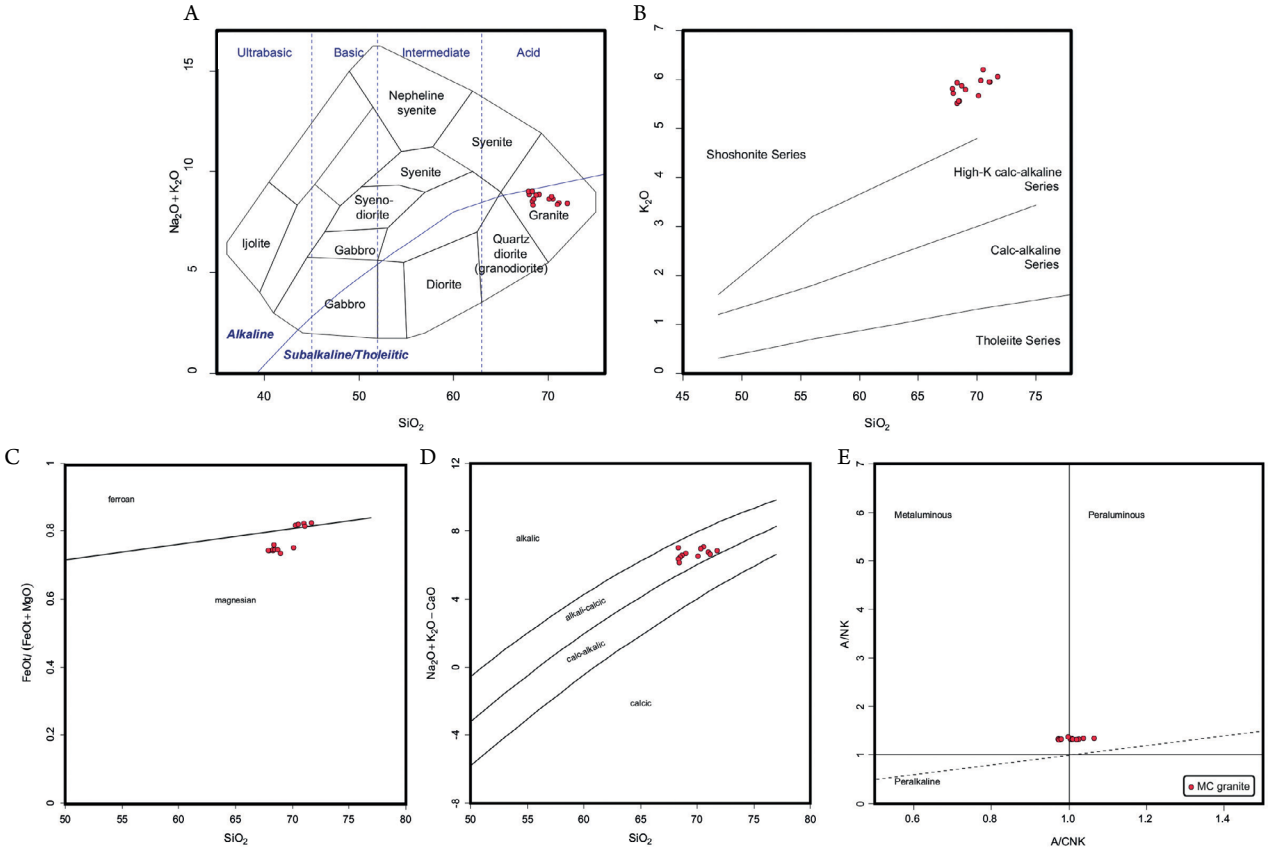

Figure 4. Geochemical classification diagrams for whole rock analyses of Morro do Coco Granite. (A) TAS (Cox *et al.* 1979); (B) K_2O *vs.* SiO_2 (Peccerillo and Taylor 1976); (C) and (D) geochemical classification diagrams ($FeO_t/FeO_t + MgO$ *vs.* SiO_2 and $Na_2O + K_2O$-CaO *vs.* SiO_2; Frost et al. 2001); (E) A/NK *vs.* A/CNK diagram (Shand 1943).

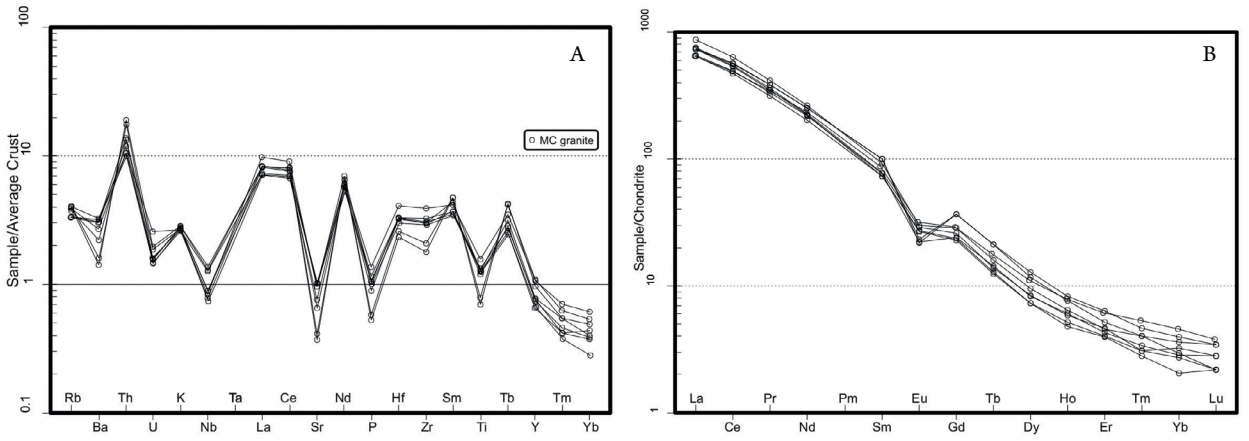

Figure 5. Multielemental and rare earth elements (REE) patterns for Morro do Coco granite samples. (A) Multielemental diagram normalized to average crust (Weaver and Tarney 1984); (B) REE pattern diagram normalized for chondrite (Boynton 1984).

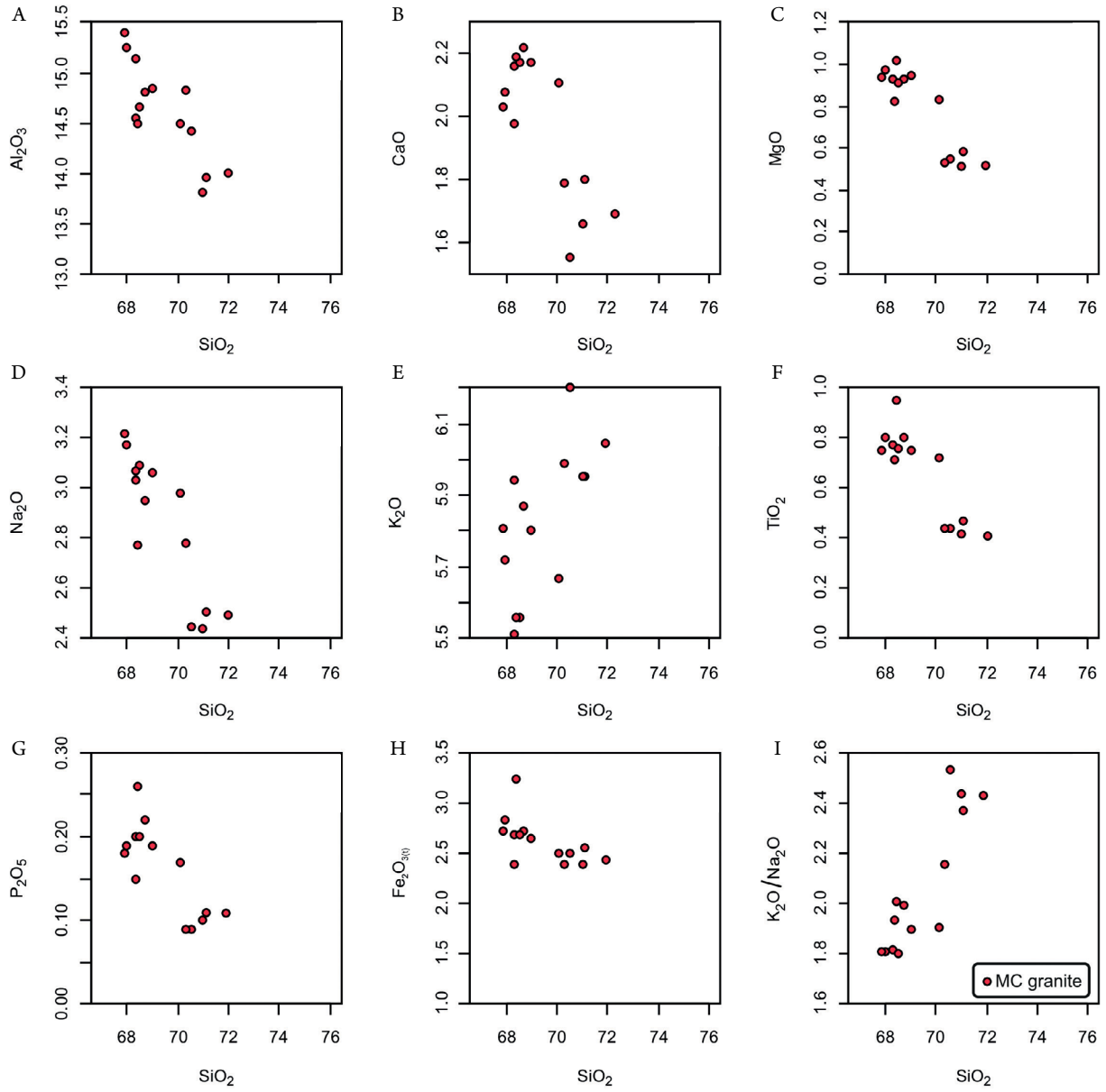

Figure 6. Binary diagrams using SiO_2 as differentiation index for major elements of Morro do Coco granite samples.

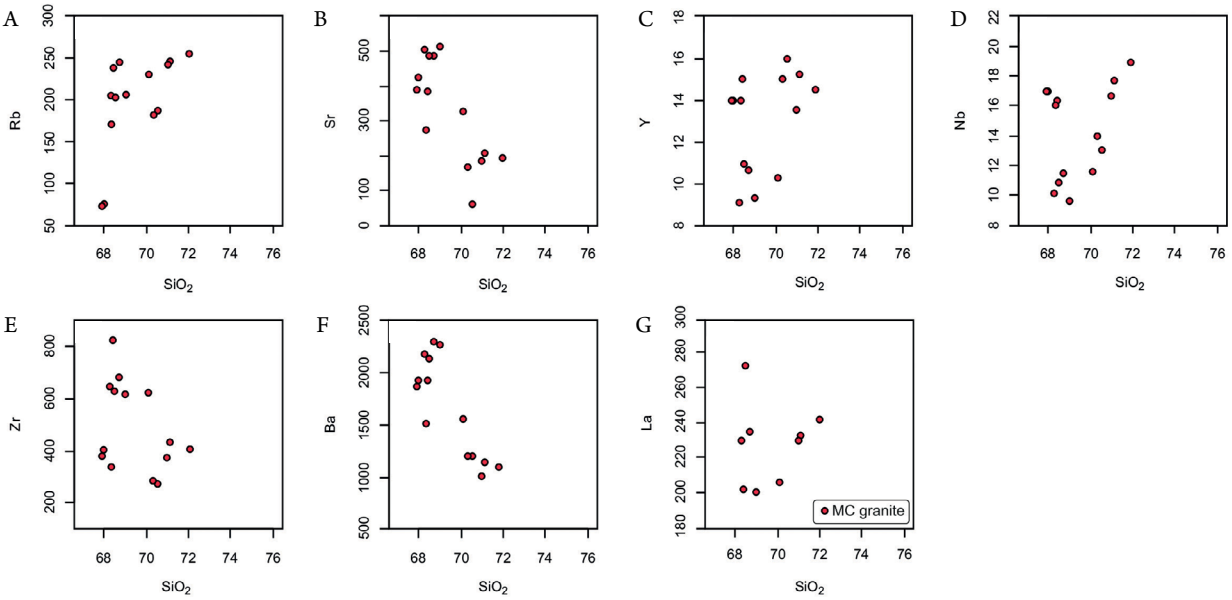

Figure 7. Binary diagrams using SiO_2 as differentiation index for selected minor and trace elements of Morro do Coco granite samples.

m3 diagrams, MC has a final probability of 83% to collisional setting, 16% to intraplate setting (CR+OI) and 1% to arc setting (CA). *Tacid* diagrams probabilities are 75% to collisional setting, 23% to arc setting and 2% to intraplate setting.

On more traditional geotectonic classification diagrams such as Rb *vs.* Y+Nb, Nb *vs.* Y, Rb *vs.* Ta+Yb and Ta *vs.* Yb of Pearce *et al.* (1984; Fig. 11), MC plots within the limit between syn-collisional granite (syn-COLG) and volcanic arc granite (VAG). Also, most of the samples plot in the post-collisional granite field (post-COLG; Pearce 1996) within the Rb *vs.* Y+Nb diagram (Fig. 11A).

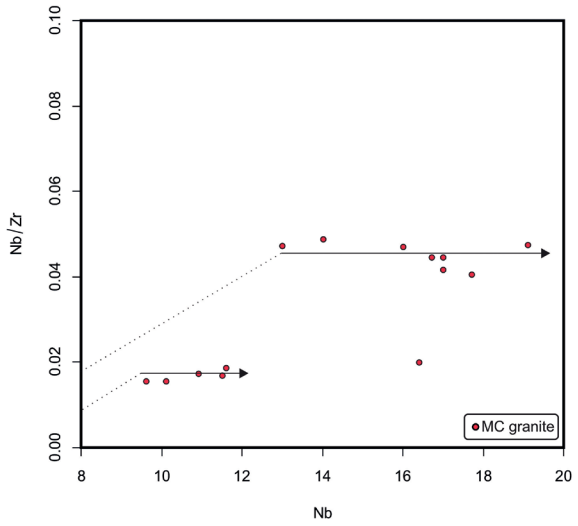

Figure 8. Nb/Zr versus Nb binary diagram plot of Morro do Coco samples. The horizontal lines represent process of fractional crystallization. The two clusters may indicate different magmatic sources.

U-Pb geochronology

Seventeen SHRIMP spots on zircon crystals from one MC sample (CLR-02C) were analyzed (Tab. 3). Crystals are prismatic, some with sub-rounded rims, and their size range from 125 to 260 μm in length and 25 to 50 μm in width, with a length/width ratio varying from 10:3 on elongated crystals to 2:1 on sharp ones. Concentric or irregular oscillatory zoning can be observed for most crystals under CL imaging, interpreted as indicating their igneous origin (Fig. 12A).

Statistical plot of all spots analyzed are shown in Figure 12B. Spots 1.1 and 4.1 yielded $^{206}Pb/^{238}U$ age of 564 and 591 Ma, respectively, being assigned as a xenocrystal, probably derived from the host rocks. Aside from these two plots, others were excluded due to high discordance degree or low Th/U ratios. Eight plots (2.1, 3.1, 5.1, 6.1, 7.1, 8.1, 13.1, 14.1) have $^{206}Pb/^{238}U$ ages between 474 and 507 Ma and yielded a concordant age of 496 ± 3 Ma with mean weighted standard deviation (MWSD) concordance of 0.63 (Fig. 12C), which we interpret as the crystallization age for the MC granite.

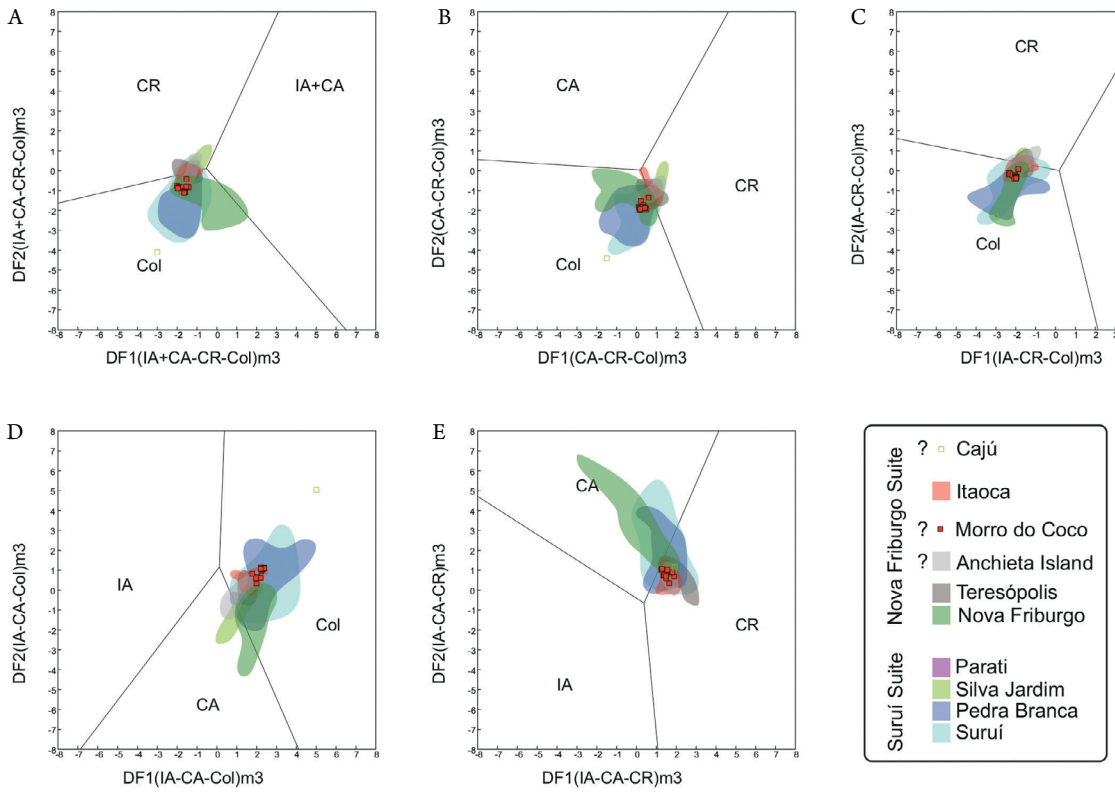

CR: Continental rift; Col: Collisional; IA: Island arc; CA: continental arc; DF1 and DF2: functions based on major elements concentrations (*cf.* Verma *et al.* 2012).

Figure 9. Multidimensional geotectonic classification diagram for acidic rocks based on major elements (*m3*, Verma *et al.* 2012) for Morro do Coco samples and a comparison with other post-collisional granitic intrusions found in Ribeira-Araçuaí Belts. Data from: Almeida (2010; Suruí), Valeriano (2012; Pedra Branca), Ribeiro (2006; Silva Jardim), Teixeira (2010; Parati), Azevedo Sobrinho *et al.* (2011; Anchieta Island), Junho (1992; Teresópolis), Potratz and Valeriano (2017; Itaoca), Bongiolo *et al.* (2016; Cajú).

Sm-Nd isotopes

Sm-Nd results for two samples (CLR-02C and CLR-07C) of the MC granite are presented in Tab. 4. The samples show $^{143}Nd/^{144}Nd$ ratios of 0.511752 and 0.511747, $\varepsilon Nd_{(496Ma)}$ ~ -9, and T_{DM} model age of 1.3 Ga (Fig. 13). Data suggest Mesoproterozoic age for parental magma extraction from its source.

DISCUSSION

The generation of MC in the late Cambrian is related to the post-collisional geodynamics that took place at the final Brasiliano orogeny, during the waning stages of the Gondwana supercontinent amalgamation. Based on the acquired data, the following sections will provide details about its geochemical and geotectonic significance and its correspondence to other similar occurrences in the Ribeira and Araçuaí belts.

Geochemistry of Morro do Coco granite

Whole-rock geochemical data classifies MC as a high-K, calc-alkaline magnesian syenogranite with metaluminous to slightly peraluminous affinity (aluminum saturation index – ASI between 0.97 and 1.06; Fig. 4, Tab. 1). Other important geochemical characteristics of the MC granite are:

- high K_2O concentrations (up to 6 wt.%, Fig. 4B) in K_2O *vs.* SiO_2 diagram;
- high $K_2O + Na_2O$ contents (around 9 wt.% Tab. 1);
- great LREE enrichment and negative Eu anomalies on the chondrite-normalized REE pattern (Fig. 5B);
- strongly negative $\varepsilon Nd_{(496)}$ of ca. -9, indicating crustal melting source.

Still, Mesoproterozoic T_{DM} ages of 1.3 Ga obtained for MC (Fig. 13, Tab. 4) are similar to model ages obtained for intermediate and mafic rocks from Várzea Alegre (Medeiros *et al.* 2000) and syn-collisional calc-alkaline granitoids from São Paulo and Minas Gerais States (Janasi *et al.* 1997), which they interpret as being related to an important crust-forming event for the area, possibly in a subduction environment associated to lithospheric mantle metasomatism. Further, magnesian granitoids are related to partial melting of continental crust under oxidizing (and probably wet) conditions (Osbourn 1959, Frost *et al.* 2001).

Variation diagrams using SiO_2 as differentiation index support that fractional crystallization took part in MC magma evolution as they present negative correlations for Al_2O_3, CaO, MgO, Na_2O, $Fe_2O_{3(t)}$ and TiO_2 and a positive one for K_2O. The depletion in CaO (and Sr) and the enrichment of K_2O (and Rb) with increasing SiO_2 contents accounts, respectively, for plagioclase fractionation and alkali-feldspar crystallization (Figs. 6 and 7). Negative Eu anomalies (δEu up to 0.35; Fig. 5B) also ascribe the removal of plagioclase from the melt by crystal fractionation or the partial melting of a source rock leaving plagioclase in the residue (*cf.* Wilson 1989). The two horizontal trend lines in the Nb *vs.* Nb/Zr binary plot (Fig. 8) are also interpreted as result of the fractional crystallization process.

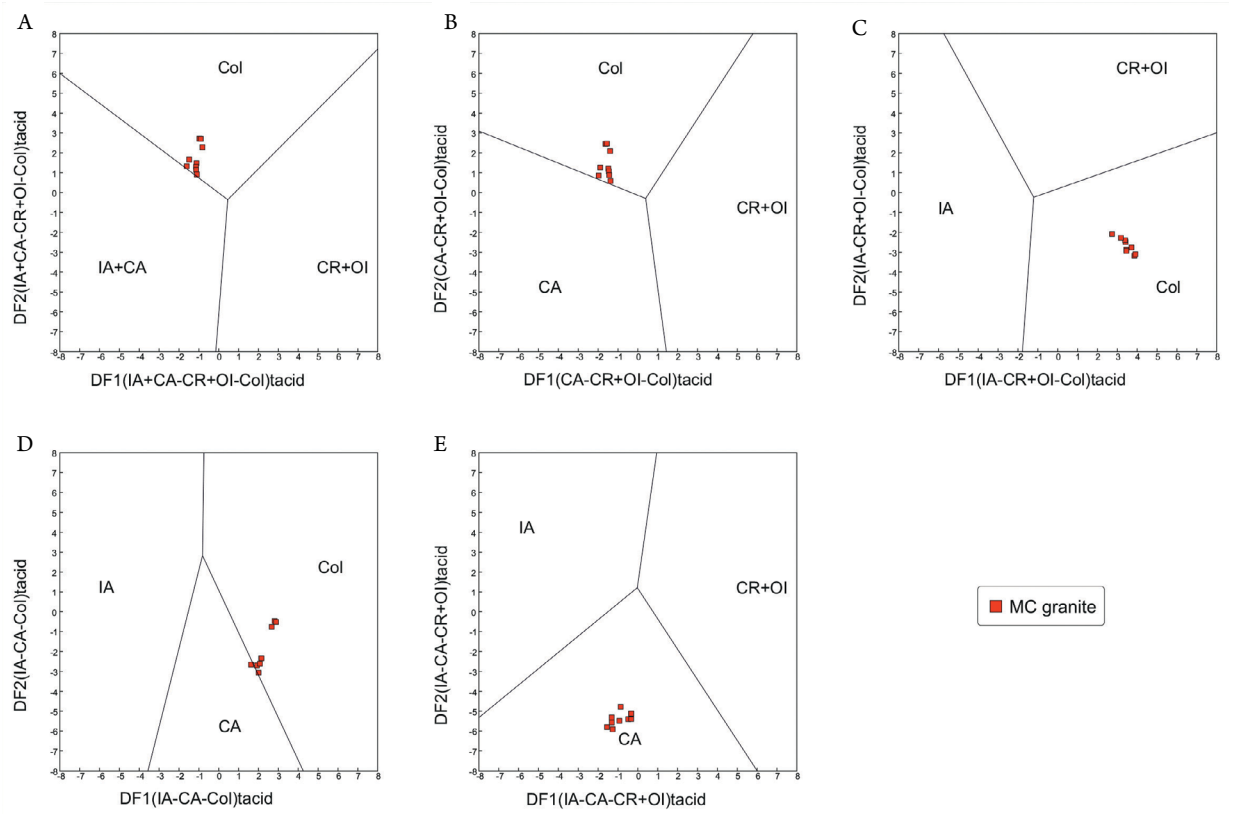

CR: Continental rift; Col: collisional; IA: island arc; CA: continental arc; OI: intraoceanic island; DF1 and DF2: functions based on trace elements concentrations (*cf.* Verma *et al.* 2013).

Figure 10. Multidimensional geotectonic classification diagram for acidic rocks based on immobile trace elements (*tacid*, Verma *et al.* 2013).

Fractional crystallization is considered an important process in the history of similar post-collisional rocks in the region, but are certainly combined, in a higher or lesser degree, with mixing between mantle-derived magmas and crustal melts (*e.g.*, Wiedemann *et al.* 1987, Mendes *et al.* 1997, 2005). This combined magma source is not evidenced in MC, as demonstrated by its petrographic and geochemical (*e.g.*, lack of association with basic rocks and slightly peraluminous affinity).

A comparison of Morro do Coco with similar occurrences

By comparing the chemical composition of MC with other similarly evolved (SiO_2 contents) post-collisional rocks of the Ribeira-Araçuaí belts (Suppl. Tab. A5), they are clearly akin. Mean values of SiO_2 (70 wt.%), Al_2O_3 (14.4 wt.%), $Fe_2O_{3(t)}$ (2.7 wt.%), CaO (1.8 wt.%) Na_2O (3.1 wt.%) and K_2O (5.8 wt.%) of the other intrusions are very alike to the concentrations of major elements in MC (Tab. 1). Only the younger Cajú granite, presenting slightly higher SiO_2 contents (up to 73 wt.%), has lower $Fe_2O_{3(t)}$ contents (1.2 wt.%).

The plot of geochemical data of post-collisional granites of the Central Ribeira Belt in the major-elements based multidimensional tectonic discrimination diagrams of Verma *et al.* (2012; Fig. 9) show they were all formed at a collisional setting, but one group (Parati, Silva Jardim, Anchieta Island, Teresópolis, Itaoca and MC) plot closer to the collisional/continental rift fields transition, while the other (Suruí, Pedra Branca and Nova Friburgo) plot scattered within the collisional field (Fig. 9A to C). Also, a different chemical behavior between these two groups is observed in the last diagram (Fig. 9E), where the latter demonstrates higher arc setting affinity. This variability may reflect heterogeneity of their magmatic sources, as there is no direct correlation between age or Suite and these geochemical signatures.

Table 2. Geotectonic setting probabilities based on the application of multidimensional diagrams to acidic rocks of Morro do Coco Granite.

Magma type, Figure name	Figure type	Total number of samples	Number of discriminated samples				
			Arc			CR+OI [x ± s] [p_CR+OI] Θ	Col [x ± s] [p_Col] Θ
			IA+CA [x ± s] [p_IA+CA] Θ	IA [x ± s] [p_IA] Θ	CA [x ± s] [p_CA] Θ		
Acid; Verma *et al.* (2012); log-ratios of all major elements	(IA+CA–CR–Col)	14	0 (0)	---	---	0 (0)	14 [0.864 ± 0.074] (0.6729–0.9931)
	(IA–CA–CR)	14	---	0 (0)	1 (0.6912)	13 [0.744 ± 0.102] (0.5708–0.8993)	---
	(IA–CA–Col)	14	---	0 (0)	0 (0)	---	14 [0.9745 ± 0.0155] (0.9456–0.9980)
	(IA–CR–Col)	14	---	0 (0)	---	0 (0)	14 [0.855 ± 0.063] (0.6885–0.9849)
	(CA–CR–Col)	14	---	---	0 (0)	0 (0)	14 [0.804 ± 0.092] (0.5695–0.9869)
Diagrams based on log-ratios of major elements	**{Σn} {Σprob} [%prob]**	70	{0} {0} [0%]	{0} {0} [0%]	{1} {0.6912} [1%]	{13} {9.6726} [16%]	{56} {48.9627} [83%]
Acid; Verma *et al.* (2013); log-ratios of immobile trace elements	(IA+CA-CR+OI-Col)	9	0 (0)	---	---	0 (0)	9 [0.730 ± 0.161] (0.5400–0.9522)
	(IA-CA-CR+OI)	9	---	0 (0)	8 [0.99999 ± 0.00000] (1.0000–1.0000)	1 (0.7504)	---
	(IA-CA-Col)	9	---	0 (0)	1 (0.5528)	---	8 [0.734 ± 0.186] (0.5182–0.9670)
	(IA-CR+OI-Col)	9	---	0 (0)	---	0 (0)	9 [0.9957 ± 0.0126] (0.9621–1.0000)
	(CA-CR+OI-Col)	9	---	---	0 (0)	0 (0)	9 [0.767 ± 0.155] (0.5582–0.9618)
Diagrams based on log-ratios of immobile trace elements	**{Σn} {Σprob} [%prob]**	45	{0} {0} [0%]	{0} {0} [0%]	{9} {8.5527} [23%]	{1} {0.7504} [2%]	{35} {28.3084} [75%]

IA: island arc; CA: continental arc; IA+CA: combined island and continental arcs, *i.e.*, arc setting; CR: continental rift; OI: ocean island; CR+OI: combined continental rift and ocean island, *i.e.*, within-plate (WP) setting; Col: collisional setting; Θ: the probability values for samples are represented by *e.g.*, (pIA+CA): probability for the combined island and continental arc setting in the first diagram; [pCol]: probability for the collision setting in the diagrams; –: ± 1 standard deviation of the probability estimates for all samples discriminated in a given tectonic setting; these are reported in [], the values are rounded mostly following the indications put forth by Verma (2005); the final rows give a synthesis of results as {Σn}, {Σprob} and [%prob], where {Σn} is the total number of samples or data points plotting in all five diagrams which is reported in the column of total number of samples, whereas the sum of samples plotting in a given tectonic field is reported in the respective tectonic field column; {Σprob}: the sum of probability values for all samples plotting in a given tectonic field, reported in the respective tectonic field column; [%prob]: the total probability of a given tectonic setting expressed in percent after assigning the probability of IA + CA to IA and CA (using weighing factors explained in Verma and Verma 2013).

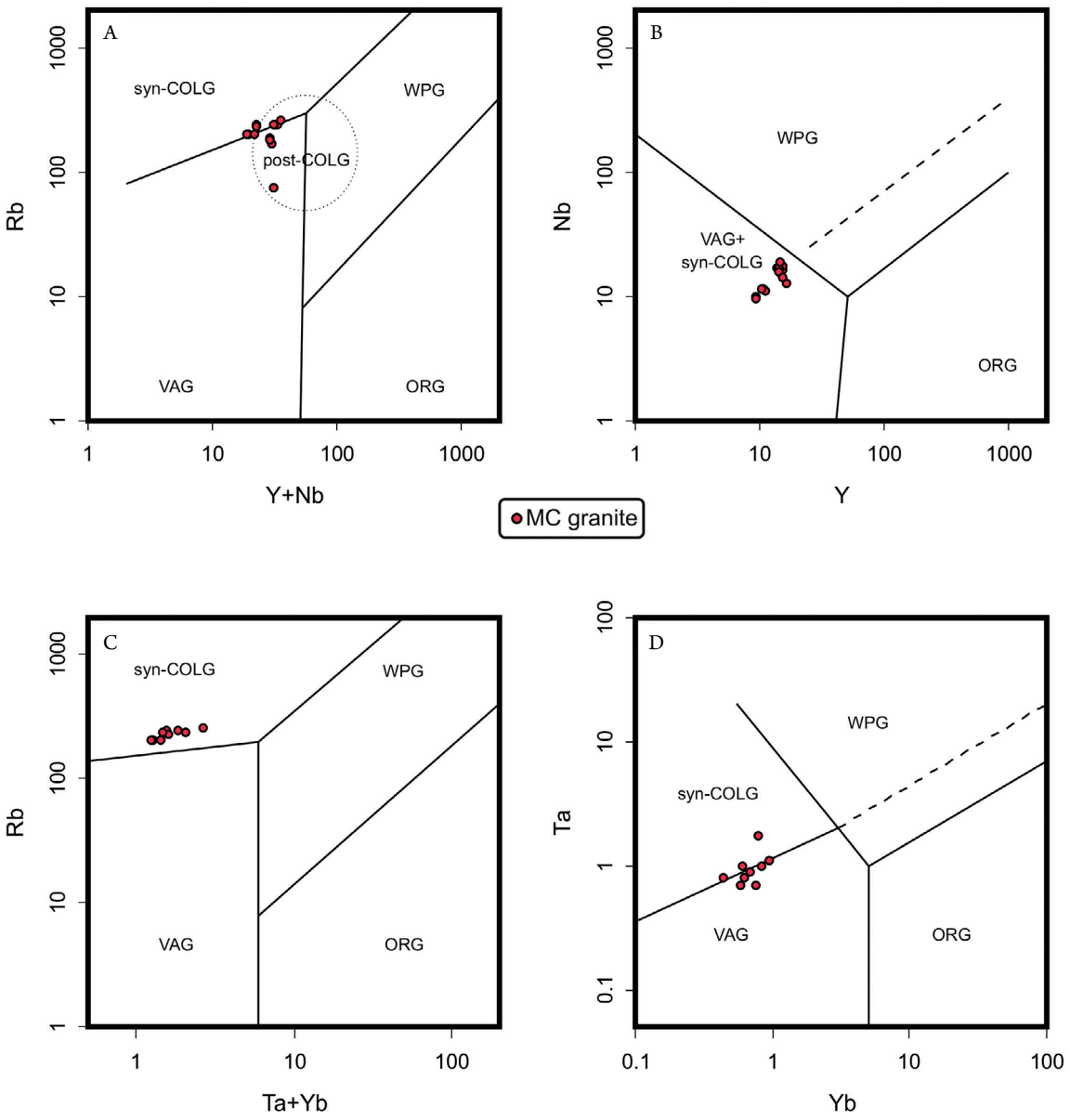

Figure 11. Pearce *et al.* (1984) granite geotectonic discriminant diagrams. (A) Rb *vs.* Y+Nb diagram (including field for post-collisional granites from Pearce 1996); (B) Nb *vs.* Y; (C) Rb *vs.* Ta + Yb; (D) Ta *vs.* Yb.

Table 3. Analytical results of sensitive high resolution ion microprobe (SHRIMP) U-Pb zircon data for the Morro do Coco Granite.

Grain spot	U (ppm)	Th (ppm)	$^{232}Th/^{238}U$	Common ^{206}Pb (%)	Rad ^{206}Pb (ppm)	$^{207}Pb/^{235}U$	error (%)	$^{206}Pb/^{238}U$	error (%)	$^{207}Pb/^{206}Pb$	error (%)	error corr	$^{206}Pb/^{238}U$ Age (Ma) 204 corr	error (1s)	$^{207}Pb/^{206}Pb$ Age (Ma) 204 corr	error (1s)	Disc (%)
MC01-1.1	94	110	1.21	0.41	7.4	0.74	3.4	0.0914	1.6	0.0587	3.0	0.467	564.0	8.5	557.5	64.7	-1
MC01-2.1	169	332	2.03	0.28	11.1	0.61	3.9	0.0763	2.7	0.0579	2.9	0.674	474.1	12.2	526.7	63.9	11
MC01-3.1	128	239	1.92	0.29	8.8	0.63	3.4	0.0796	1.6	0.0574	3.0	0.458	493.8	7.4	508.1	66.5	3
MC01-4.1	237	72	0.32	0.00	19.6	0.79	1.8	0.0960	1.5	0.0597	1.0	0.827	591.1	8.3	594.4	21.7	1
MC01-5.1	219	227	1.07	0.03	15.2	0.64	2.6	0.0807	1.7	0.0577	2.0	0.645	500.2	8.1	516.6	43.6	3
MC01-6.1	132	216	1.68	0.47	9	0.63	3.5	0.0791	2.1	0.0581	2.8	0.597	490.5	9.9	533.1	61.5	9
MC01-7.1	142	258	1.87	-0.07	9.6	0.62	4.3	0.0785	1.6	0.0568	4.0	0.372	487.1	7.5	485.0	88.4	0
MC01-8.1	219	305	1.44	1.05	15.5	0.64	4.3	0.0812	1.5	0.0573	4.0	0.349	503.4	7.3	504.6	89.6	0
MC01-9.1	232	566	2.52	0.50	15.1	0.62	3.7	0.0753	2.0	0.0593	3.1	0.540	468.2	8.9	576.6	67.0	23
MC01-10.1	128	266	2.14	0.48	8.7	0.64	2.8	0.0784	1.5	0.0589	2.3	0.554	486.8	7.2	563.4	50.5	16
MC01-11.1	155	293	1.96	0.23	10.6	0.64	2.3	0.0793	1.5	0.0588	1.7	0.670	492.0	7.2	559.5	36.5	14
MC01-12.1	145	298	2.12	0.51	10.3	0.65	3.4	0.0824	1.5	0.0575	3.0	0.448	510.5	7.5	509.8	67.1	0
MC01-13.1	179	397	2.29	0.43	12.1	0.62	3.1	0.0785	1.5	0.0571	2.7	0.490	487.1	7.1	495.5	59.1	2
MC01-14.1	180	396	2.28	0.43	12.5	0.64	3.0	0.0805	1.6	0.0581	2.5	0.528	498.8	7.5	532.5	55.1	7
MC01-15.1	209	447	2.21	-0.09	14.2	0.65	2.0	0.0791	1.6	0.0601	1.2	0.813	490.6	7.6	605.8	24.9	23
MC01-16.1	200	370	1.91	0.76	13.6	0.64	3.9	0.0783	1.5	0.0593	3.6	0.386	486.0	7.1	578.7	78.6	19
MC01-17.1	451	70	0.16	0.01	31.7	0.65	1.7	0.0819	1.4	0.0572	0.8	0.876	507.3	7.1	500.4	17.6	-1

Trace-elements-based tectonic classification diagrams corroborate that MC was formed at a collisional/post-collisional setting but, in this case, some samples show arc affinity (Figs. 10 and 11), as noted by Pearce (1996). As stated by Frost *et al.* (2001), the trace-elements compositions of post-collisional granitoids are highly controlled by melting source and crystallization history, rather than the tectonic environment, as they can be derived from different types of sources depending on the composition of the thickened crust. Thus, this arc-related geochemical signature of MC could be inherited from the melting source.

Incipient deformation is mostly described in the Suruí Suite (Valeriano *et al.* 2017). Undulose extinction in quartz crystals and development of myrmekite in plagioclase (Fig. 3G-3J) may indicate solid-state deformation (*cf.* Vernon *et al.* 2004) in the MC granite. Also, alkali-feldspar recrystallization (Fig. 3K-3L) indicates P-T arrangement of at least 480ºC at 4 kb conditions (Voll 1976, Altenberger *et al.* 1987) during MC emplacement. This is the expected temperature for the study area in the post-collisional stage of the Ribeira orogen at 495 Ma, using cooling rates of 10ºC/Ma after the metamorphic peak at 525 Ma (ca. 780°C and 9 kb; Schmitt *et al.* 2004) near the study area. Thus, incipient deformation observed in MC and other post-collisional intrusion of the Ribeira orogeny might represent the rheological behavior of their magmas under advanced crystallization (35–65%; *e.g.*, Fernandez and Gasquet 1994).

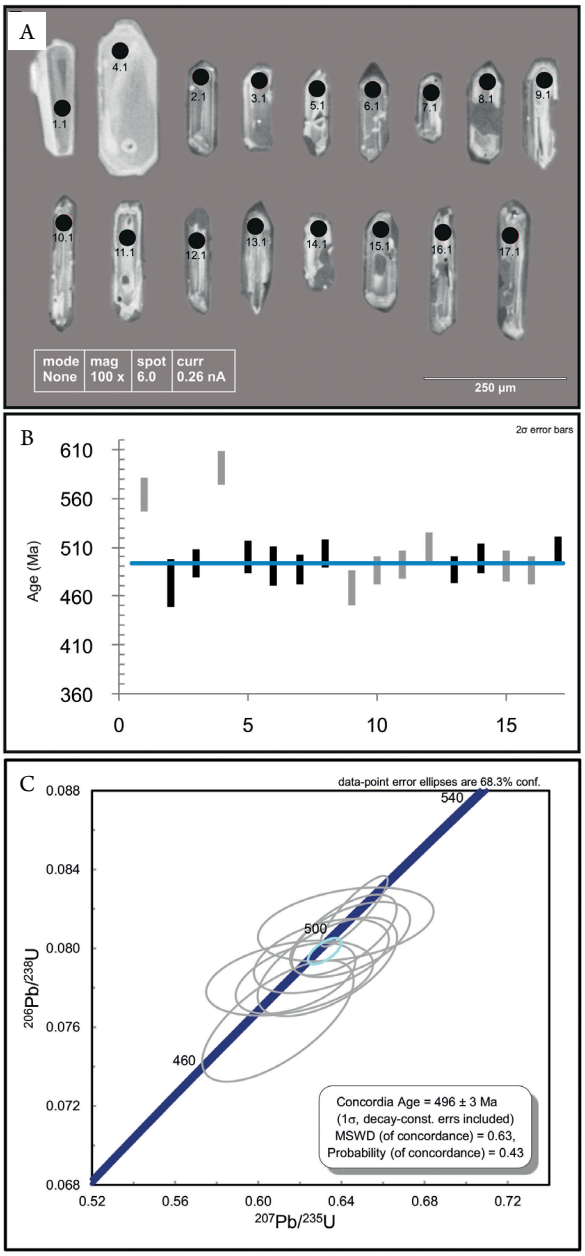

Figure 12. Geocrhonology of Morro do Coco granite. (A) Cathodoluminescence images from zircon crystals of Morro do Coco granite; (B) statistical plot of all ages of analyzed spots with error bar of 2σ. Only the spots represented by black bars were used to calculate the concordant age; (C) U-Pb sensitive high resolution ion microprobe (SHRIMP) Concordia diagram showing only nine selected spots.

Post-collisional age span in southeastern Brazil

The current subdivision of the Cambro-Ordovician granitic intrusions of the Ribeira Belt into two Suites (*i.e.*, Suruí and Nova Friburgo) suggests two pulses of magmatism during the post-collisional stage of the Brasiliano orogeny. The Suruí and Nova Friburgo Suites are distinguished over age, structural and geomorphological criteria. According to Valeriano *et al.* (2017), Suruí Suite (~510 Ma) occurs mostly as stocks and batholiths and show superimposed weak ductile deformation; while Nova Friburgo Suite (~485 Ma) granitoids are generally represented by tabular intrusions without clear signs of ductile deformation.

Nevertheless, by comparing these ages and extending this comparison to the South Ribeira and Araçuaí belts, a broader distribution can be observed if we consider analytical errors (Fig. 14, Tab. 5). In Fact, only Pedra Branca, Suruí, Santa Angélica and Pedra Azul granitoids clearly cluster as older representants of this magmatism, and Cajú as the youngest intrusion (ca. 454 Ma; Bongiolo *et al.* 2016). The other intrusions span intermediately, at ca. 495-475 Ma, which could either indicate three pulses of magmatism (515, 495 and 455 Ma) or a continuous event from 515 to 475 Ma with an interval of 20 Ma to a second pulse at ca. 455 Ma.

The MC granites have crystallization age of 496 ± 3 Ma, similarly to those of the Nova Friburgo Suite crystallization (ca. 485 Ma; Fig. 14, Tab. 5). Based on geochemical characteristics, age and tabular geometry, MC is interpreted here as belonging to the Nova Friburgo Suite.

Table 4. Sm-Nd isotopic data for the Morro do Coco Granite.

Sample	Sm (ppm)	Nd (ppm)	$^{147}Sm/^{144}Nd$	error (2s)	$(^{143}Nd/^{144}Nd)_0$	$\varepsilon Nd_{(0)}$	$(^{143}Nd/^{144}Nd)_t$	$\varepsilon Nd_{(t)}$	T_{DM} (Ga)	t (Ga)
CLR-02C	16	150	0.067880	0.00040	0.511752	-17.3	0.511532	-9.15	1.35	0.5
CLR-07C	16	113	0.064385	0.00038	0.511747	-17.4	0.511538	-9.03	1.32	0.5

Post-collisional Ribeira *vs.* Araçuaí belts and current geodynamic models

The petrographic and geochemical characteristics of MC are indicative of granites formed by processes associated to delamination of overthickened crust (Frost *et al.* 2001), which is one of the most accepted geodynamic models proposed for the Cambro-Ordovician magmatism at the Ribeira-Araçuaí belts (Heilbron and Machado 2003, Pedrosa-Soares *et al.* 2008). Break-off of subducted oceanic lithosphere is also proposed as a triggering mechanism for this post-collisional magmatism (Söllner *et al.* 1987, 2000). In fact, both processes could have taken place synchronously. Other possible mechanism is the onset of a hotspot due to destabilization of the asthenospheric mantle after orogenic collapse, proposed by De Campos *et al.* (2016) to explain post-collisional bimodal intrusive bodies such as Mimoso do Sul, Buarama and Várzea Alegre (ca. 499 to 480 Ma; Söllner *et al.* 2000, Mendes *et al.* 2005) at the Araçuaí Belt.

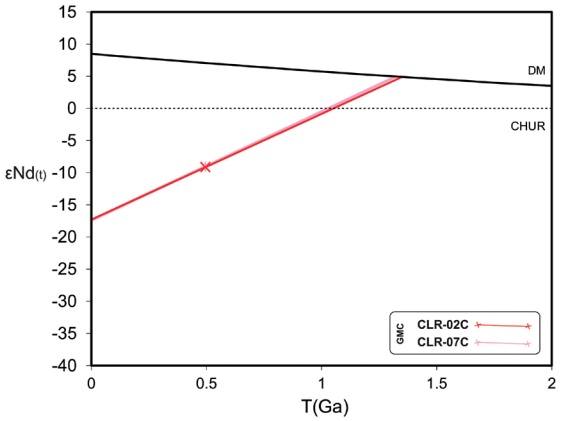

Figure 13. εNd *vs.* time (Ga) evolution diagram for two samples (CLR-02C and CLR-07C) of the Morro do Coco granite.

These models highlight extensive melting of the lower continental crust driven by asthenospheric mantle uplift and the production of mantle-derived tholeiitic magmas, which is not observed in MC, as it comprises a homogenous granitic body with no evidence of associated mafic rocks. Either way, these continental scale processes could have provided the necessary heat to partially melt the continental crust and generate MC.

Post-collisional intrusions in Southern Ribeira Belt (*e.g.*, Anchieta Island quartz-monzonite; Azevedo Sobrinho *et al.* 2011) and in Northern Ribeira, and Southern Araçuaí belts transition zone, Espírito Santo State (*e.g.*, Mimoso do Sul, Santa Angélica, Castelo, Pedra Azul and Várzea Alegre) are

Table 5. Geochronological data compilation of some of the Cambro-Ordovician intrusive bodies in the Ribeira and Araçuaí belts.

Unit	Suite	Age	Error	Method		Reference
Guarujá-Santos	-	497	7	U-Pb SHRIMP	zircon	Janasi *et al.* (2015)
Anchieta	-	499.7	5.9	LA-ICPMS	zircon	Azevedo Sobrinho *et al.* (2011)
Parati	Suruí	500	-	U-Pb	zircon	Ludka *et al.* (2006)
Pedra Branca	Suruí	513	5	ID-TIMS	zircon	Heilbron and Machado (2003)
Vila Dois Rios	Suruí	?	-	-	-	Fernandes (2000); Eirado *et al.* (2006)
Suruí	Suruí	512	7	LA-ICPMS	zircon	Valeriano *et al.* (2011)
Silva Jardim	Suruí	505	2	LA-ICPMS	zircon	Moraes (2009)
Mangaratiba/Mambucaba	Nova Friburgo	492	15	ID-TIMS	titanite	Machado *et al.* (1996)
Favela	Nova Friburgo	482	6	LA-ICPMS	zircon	Heilbron and Machado (2003)
Andorinha	Nova Friburgo	490	9	LA-ICPMS	zircon	Valeriano *et al.* (2011)
Teresópolis/Frades	Nova Friburgo	481	6	LA-ICPMS	zircon	Valeriano *et al.* (2011)
Nova Friburgo	Nova Friburgo	489	4	LA-ICPMS	titanite	Valeriano *et al.* (2011)
Conselheiro Paulino	Nova Friburgo	?	-	-	-	Pacheco (2010)
São José do Ribeirão	Nova Friburgo	?	-	-	-	Mendes *et al.* (2002)
Sana	Nova Friburgo	491	10	LA-ICPMS	zircon	Valeriano *et al.* (2011)
São Pedro de Lumiar	Nova Friburgo	490	-	Inferred	-	Mendes *et al.* (2011)
Itaoca	Nova Friburgo	476	2	ID-TIMS	monazite	Neto *et al.* (2014)
Morro do Coco	Nova Friburgo	496	3	U-Pb SHRIMP	zircon	This work
Cajú	-	454	5	U-Pb SHRIMP	zircon	Bongiolo *et al.* (2016)
Mimoso do Sul	-	495	5	U-Pb	zircon	Söllner *et al.* (2000)
Santa Angélica	-	513	8	U-Pb	zircon	Söllner *et al.* (2000)
Buarama	-	480	4	U-Pb	zircon	Söllner *et al.* (2000)
Pedra Azul	-	536	31	Whole-rock Rb-Sr	-	Platzer (1997)
Várzea Alegre	-	499	5	ID-TIMS	zircon	Mendes *et al.* (2005)

SHRIMP: sensitive high resolution ion microprobe; LA-ICPMS: laser ablation inductively coupled plasma mass spectromete; ID-TIMS: thermal ionization mass spectrometry isotopic dilution:

interpreted to result from the interaction between mantle-derived magmas and partial melting of the lower crust (De Campos *et al.* 2004, 2016, Azevedo Sobrinho *et al.* 2011). Regarding the latter, De Campos *et al.* (2016) emphasize the complexity and uniqueness of their internal structures and the broadness of magma mixing/mingling evidences, and that they represent the roots of these plutons exposed by deep erosion levels combined with high vertical exposures, which is supported by geobarometric studies that point to intrusions depths around 20 km for these rocks (> 6 kb; Mendes *et al.* 1997, Medeiros *et al.* 2001).

However, MC and other Cambro-Ordovician intrusive bodies emplaced at the central Ribeira Belt, Rio de Janeiro State, seem to represent a shallower portion of the continental crust, with "undeformed" high-K calc-alkaline to alkali-calcic mainly metaluminous granites and lesser amounts of quartz-monzonites (*e.g.*, Suruí, Pedra Branca, Parati, Silva Jardim, Vila Dois Rios, Nova Friburgo, Mangaratiba, Favela, Andorinha, Teresópolis, Sana, São Pedro, Itaoca, etc.). Post-collisional pegmatites that crop out in the CFTD and are related to the Cajú granite were emplaced at shallow crustal levels, between 1.7 to 3.5 km (Bongiolo *et al.* 2016).

Most of these granitoids carry gabbroic, dioritic and quartz-dioritic microgranular enclaves (Valeriano *et al.* 2016) which could be related to primitive magma sources, but no mafic enclaves/xenoliths were observed in MC so far. Despite the occurrence of scarce structures interpreted as magma mingling (*e.g.*, Mendes *et al.* 2002, Pacheco 2010, Valeriano *et al.* 2017), the post-collisional granitoid intrusions of the central Ribeira Belt do not display clear signs of interaction with more primitive (basic) magmas as it is observed in the Araçuaí Belt.

Considering that the CFTD was formed by a west-dipping subduction prior to the Buzios orogeny, this event could have provided extra heating of the upper plate (Costeiro Domain). Thus, the more significant crustal contribution concentrated at the central Ribeira Belt, along with the larger number of known post-collisional intrusions in this sector (Fig. 1), could be related to their proximity to the CFTD. The alignment of post-collisional magmatism along a NE/SW-trending corridor through the Ribeira Belt is concordant with preexisting NE/SW dextral shear zones that could have supported the ascent of post-collisional magmatism after the Búzios orogeny (Schmitt *et al.* 2016, Martins *et al.* 2016).

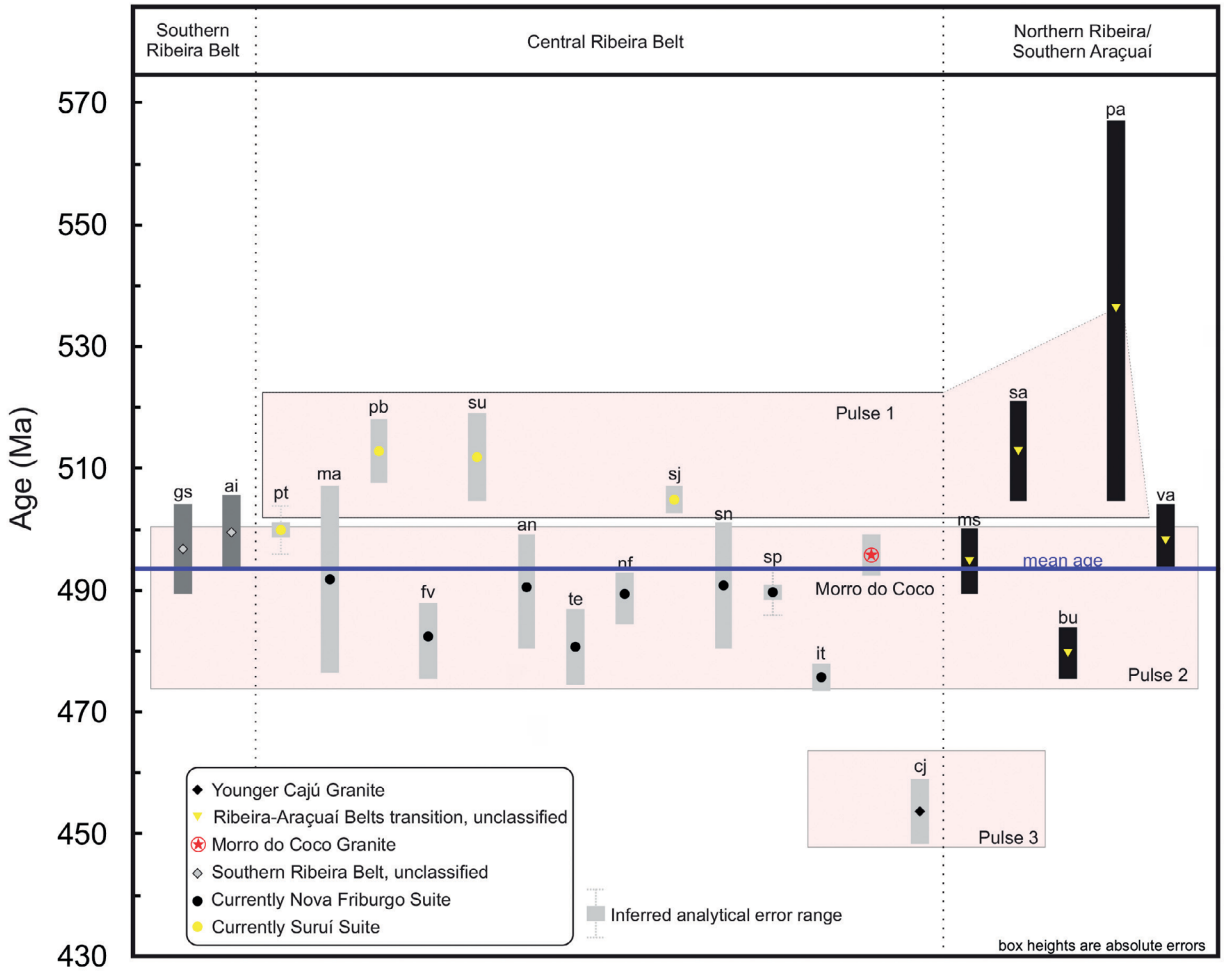

gs: Guarujá-Santos; ai: Anchieta Island; pt: Parati; ma: Mangaratiba/Mambucaba; pb: Pedra Branca; fv: Favela; su: Suruí; an: Andorinha; te: Teresópolis/ Frades; nf: Nova Friburgo; sj: Silva Jardim; sn: Sana; sp: São Pedro de Lumiar; it: Itaoca; mc: Morro do Coco; cj: Cajú; ms: Mimoso do Sul; sa: Santa Angélica; bu: Buarama; pa: Pedra Azul; va: Várzea Alegre.

Figure 14. Plot of the geochronological data compilation for the Cambro-Ordovician intrusive bodies at the Ribeira-Araçuaí belts from Southern Ribeira Belt to Southern Araçuaí Belt. The Parati and São Pedro de Lumiar error bars are inferred. The Pedra Azul has a very imprecise age due to the methodology used (whole-rock Rb-Sr). Data References are shown in Table 5.

CONCLUSIONS

Based on the presented investigation, our study of the post-collisional MC Granite indicates that:

- The MC granite is a homogeneous, nearly undeformed, tabular syenogranite that was emplaced at the final stages of continental amalgamation at the central Ribeira Belt, during the late Cambrian. U-Pb zircon ages yields a crystallization age of 496 ± 3 Ma;
- As MC has no evident field or petrographic association to basic/ultrabasic rocks and is classified as an evolved high-K calc-alkaline rock, it is reasonable to assume a major magmatic crustal source, which is stressed by the strong negative εNd value;
- MC exhibits negative correlations of Al_2O_3, CaO, MgO, $Fe_2O_{3(t)}$ and TiO_2 along with positive correlation of K_2O with increasing SiO_2 contents, strong Eu anomalies, and Nb/Zr *vs.* Nb plots favoring the fractional crystallization process;
- The comparison of MC with other Cambro-Ordovician granitic intrusions of the central Ribeira Belt present similar geochemical characteristics. Based on geochemistry, morphology and geochronology we classify MC as belonging to the Nova Friburgo Suite;
- The age distribution of the main post-collisional magmatism in Central Ribeira Belt spans between 513 to 454 Ma and could be divided into three main pulses of magmatism: 515, 495 and 455 Ma.

ACKNOWLEDGEMENTS

F.R.A. Bione thanks the Conselho Nacional de Desenvolvimento Científico e Tecnológico (CNPq) for the MSc. scholarship in Brazil. This work was mostly funded by the Fundação de Amparo à Pesquisa do Estado do Rio de Janeiro (FAPERJ) (grant #E-26/111.752/2010 – APQ1). The Programa de Apoio à Pós-Graduação (PROAP) is also acknowledged for financing part of the geochemical analyses. The authors also acknowledge the Centro de Tecnologia Mineral (CETEM) for all the support during sample preparations and two anonymous reviewers of the *Brazilian Journal of Geology* for their comments that improved the quality of the manuscript.

ARTICLE INFORMATION

Manuscript ID: 20190010. Received on: 02/19/2019. Approved on: 05/24/2019.

Author F. B. contributed with the geological mapping and sampling, the petrography, wrote all items of the paper since its first version, and treated and interpreted all the data; author E. B. also contributed with the mapping and sampling, helped with the writing of all items of the paper and data interpretation; author J. M. helped with the geological mapping, petrography, chemical analyses and helped improve the manuscript with some revision and suggestions; author C. R. helped in the geological mapping, sampling, petrography and geochemical data interpretation.

Competing interests: The authors declare no competing interests.

REFERENCES

Almeida G.A. 2010. *Revisão Petroquímica dos Granitóides Pós-Colisionais ocorrentes na Folha Baía de Guanabara (1:100000), RJ, Brasil*. Undergraduate thesis, Instituto de Agronomia, Departamento de Geociências, Universidade Federal Rural do Rio de Janeiro, Rio de Janeiro, 86 p.

Altenberger U., Hamm N., Kruhl J. 1987. Movements and metamorphism north of the Insubric Line between Val Loana and Val d'Ossola (Italy). *Jahrbuch der Geologischen Bundesanstalt (Austria)*, **130**:365-374.

Azevedo Sobrinho J.M., Janasi V.A., Simonetti A., Heaman L.M., Santoro J., Diniz H.N. 2011. The Ilha Anchieta Quartz Monzonite: the southernmost expression of ca. 500 Ma post-collisional magmatism in the Ribeira Belt. *Anais da Academia Brasileira de Ciências*, **83**(3):891-906. http://dx.doi.org/10.1590/S0001-37652011000300010

Bento dos Santos T.M., Munhá J., Tassinari C., Fonseca P., Dias Neto C. 2010. Thermochronology of central Ribeira Fold Belt, SE Brazil: petrological and geochronological evidence for high-temperature maintenance during Western Gondwana amalgamation. *Precambrian Research*, **180**(3-4):285-298. http://dx.doi.org/10.1016/j.precamres.2010.05.002

Bento dos Santos T.M., Tassinari C.C.G., Fonseca P.E. 2015. Diachronic collision, slab break-off and long-term high thermal flux in the Brasiliano-Pan-African orogeny: implications for the geodynamic evolution of the Mantiqueira Province. *Precambrian Research*, **260**:1-22. http://dx.doi.org/10.1016/j.precamres.2014.12.018

Black L.P., Kamo S.L., Allen C.M., Aleinikoff J.N., Davis D.W., Korsch R.J., Foudoulis C. 2003. TEMORA 1: a new zircon standard for Phanerozoic U–Pb geochronology. *Chemical Geology*, **200**(1-2):155-170.

Bongiolo E.M., Renac C., Piza P.D., Schmitt R.S., Mexias A.S. 2016. Origin of pegmatites and fluids at Ponta Negra (RJ, Brazil) during late-to post-collisional stages of the Gondwana Assembly. *Lithos*, **240-243**:259-275. http://dx.doi.org/10.1016/j.lithos.2015.11.015

Boynton W.V. 1984. Geochemistry of the rare earth elements, Meteorite studies. In: Henderson P. (ed.). *Rare earth element Geochemistry*. Amsterdam: Elsevier, p. 63-14.

Brito Neves B.B., Fuck R.A., Pimentel M.M. 2014. The Brasiliano collage in South America: a review. *Brazilian Journal of Geology*, **44**(3):493-518. http://dx.doi.org/10.5327/Z2317-4889201400030010

Campbell I.H., Stepanov A.S., Liang H.-Y., Allen C.M., Norman M.D., Zhang Y.-Q., Xie Y.-W. 2014. The origin of shoshonites: new insights from the Tertiary high-potassium intrusions of eastern Tibet. *Contributions to Mineralogy and Petrology*, **167**:983-1005. https://doi.org/10.1007/s00410-014-0983-9

Claué-Long J.C., Compston W., Roberts J., Fanning C.M. 1995. Two carboniferous ages: 819 a comparison of SHRIMP zircon dating with conventional zircon ages and Ar/Ar analysis. In: Berggren WA, Kent DV, Aubrey MP, Hardenbol J. (eds.). *Geochronology Time Scales and Global Stratigraphic Correlation*. United Kingdom: SEPM Special Publication, **4**, p. 3-21.

Cox K.G., Bell J.D., Pankhurst R.J. 1979. *The Interpretation of Igneous Rocks*. London: George Allen and Unwin, 450 p.

Cunha P.R.C., Melo J.H.G., Silva B.O. 2007. Bacia do Amazonas. *Cartas Estratigráficas: Boletim de Geociências da Petrobras*, Rio de Janeiro, **15**(2):227-251.

De Campos C., Medeiros S., Mendes J., Pedrosa-Soares A.C., Dussin I., Ludka I., Dantas E. 2016. Cambro-Ordovician magmatism in the Araçuaí belt (SE Brazil): snapshots from a post-collisional event. *Journal of South American Earth Sciences*, **68**:248-268. https://doi.org/10.1016/j.jsames.2015.11.016

De Campos C.P., Mendes J.C., Ludka I.P., Medeiros S.R., Moura J.C., Wallfass C. 2004. A review of the Brasiliano magmatism in southern Espírito Santo, Brazil, with emphasis on post-collisional magmatism. *Journal of the Virtual Explorer*, **17**:1-39. https://doi.org/10.3809/jvirtex.2004.00106

DePaolo D.J. 1981. A neodymium and strontium isotopic study of the Mesozoic calc-alkaline granitic batholiths of the Sierra Nevada and Peninsular Ranges, California. *Journal of Geophysical Research*, **86**(B11):10470-10488. https://doi.org/10.1029/JB086iB11p10470

Eirado L.G., Heilbron M., Almeida J.C.H. 2006. Os terrenos tectônicos da Faixa Ribeira na Serra da Bocaina e na Baía da Ilha Grande, sudeste do Brasil. *Revista Brasileira de Geociências*, **36**(3):426-436.

Eirado L.G., Heilbron M., Ragatky C.D., Tupinambá, M., Peixoto, C. 2017. *Unidades Metassedimentares Neoproterozoicas da Faixa Ribeira no Estado do Rio de Janeiro*. Geologia e recursos minerais do estado do Rio de Janeiro: Texto Explicativo dos Mapas Geológico e de Recursos Minerais do Estado do Rio de Janeiro. Rio de Janeiro: CPRM, p. 45-60.

Fernandes G.A. 2000. *Contribuição ao Entendimento Geológico do Terreno Oriental da Faixa Ribeira na Baía da Ilha Grande, litoral sul fluminense, RJ*. Dissertation, Faculdade de Geologia, Universidade do Estado do Rio de Janeiro, Rio de Janeiro, 138 p.

Fernandes G.L.F., Schmitt R.S., Bongiolo E.M., Basei M.A.S., Mendes J.C. 2015. Unraveling the tectonic evolution of a Neoproterozoic-Cambrian active margin in the Ribeira Orogen (SE Brazil): U-Pb and Lu-Hf provenance data. *Precambrian Research*, **226**:337-360. http://dx.doi.org/10.1016/j.precamres.2015.05.017

Fernandez A.N., Gasquet D.R. 1994. Relative rheological evolution of chemically contrasted coeval magmas: example of the Tichka plutonic complex (Morocco). *Contributions to Mineralogy and Petrology*, **116**(3):316-326. https://doi.org/10.1007/BF00306500

Fonseca M.J.G., Silva Z.C.G., Campos D.A., Tosatto P. 1979. *Folhas do Rio de Janeiro, Vitória e Iguape*. Texto explicativo e Mapa. Brasília: DNPM, 239 p.

Frost B.R., Barnes C.G., Collins W.J., Arculus R.J., Ellis D.J., Frost C.D. 2001. A geochemical classification for granitic rocks. *Journal of Petrology*, **42**(11):2033-2048.

Hamilton P.H., O'Nions R.K., Bridgewater D., Nutman A. 1983. Sm-Nd studies of Archean metasediments and metavolcanics from West Greenland and their implications for the Earth's early history. *Earth and Planetary Science Letters*, **62**(2):263-272. https://doi.org/10.1016/0012-821X(83)90089-4

Heilbron M., Machado N. 2003. Timing of terrane accretion in the Neoproterozoic-Eopaleozoic Ribeira orogen (SE Brazil). *Precambrian Research*, **125**(1-2):87-112. http://dx.doi.org/10.1016/S0301-9268(03)00082-2

Heilbron M., Mohriak W., Valeriano C.M., Milani E., Almeida, J.C.H., Tupinambá M. 2000. From collision to extension: the roots of the South-eastern continental margin of Brazil. *In*: Talwani M. (ed.), *Atlantic Rifts and Continental Margin*. AGU Geophysical Monograph Series, **115**. 354 p.

Heilbron M., Pedrosa-Soares A.C., Campos Neto M.C., Silva L.C., Trouw R.A.J., Janasi V.A. 2004. Província Mantiqueira. *In*: Mantesso-Neto V., Bartorelli, A., Carneiro C., Dal Ré, Brito-Neves B.B. (eds.), *Geologia do Continente Sul-Americano:* Evolução da Obra de Fernando Flávio Marques de Almeida. São Paulo, Beca, p. 203-235.

Heilbron M., Tupinambá M., Valeriano C.M., Armstrong R., Silva L.G.E., Melo R.S., Simonetti A., Pedrosa-Soares A.C., Machado N. 2013. The Serra da Bolívia complex: the record of a new Neoproterozoic arc-related unit at Ribeira belt. *Precambrian Research*, **238**:158-175. http://dx.doi.org/10.1016/j.precamres.2013.09.014

Heilbron M., Valeriano C.M., Tassinari C.C.G., Almeida J.C.H., Tupinambá M., Siga Junior O., Trouw R.A.J. 2008. Correlation of Neoproterozoic terranes between Ribeira Belt, SE Brazil and its African counterpart: comparative tectonic evolution and open questions. In: Pankhurst R.J., Trouw R.A.J., Brito Neves B.B., de Wit M.J. (eds.), *West Gondwana:* Pre-Cenozoic Correlations Across the South Atlantic Region. Geological Society of London, Special Publication, **295**:211-237.

Hibbard M.J. 1995. *Petrography to Petrogenesis*. New Jersey, Prentice Hall, 608 p.

Janasi V.A., Haddad R.C., Vlach S.R.F. 1997. Comments on the Sm-Nd isotope systematics of calc-alkaline granitoids from Pinhal-Ipiuna batholith (São Paulo and Minas Gerais, Brazil). *In*: South American Symposium on Isotope Geology, Campos do Jordão. *Extended Abstract…* , 147-150.

Janasi V.A., Vasconcellos A.C.B.C., Siga Júnior O., Sato K., Machado F.B., Martins L., Garcia M.G.M. 2015. In situ U-Pb dating and Hf isotope geochemistry of zircons from granites of the Costeiro Domain, SE Brazil: timing and source contrasts with neighboring terranes of the Ribeira Belt. *In*: Hutton Symposium on Granites and Related Rocks, 8., Florianópolis. *Annals…* , v. 1, p. 69.

Janoušek V., Farrow C.M., Erban V. 2006. Interpretation of whole-rock geochemical data in igneous geochemistry: introducing Geochemical Data Toolkit (GCDkit). *Journal of Petrology*, **47**(6):1255-1259. https://doi.org/10.1093/petrology/egl013

Junho M.C.B. 1992. *Contribuição à petrologia dos maciços graníticos da Pedra Branca, Frades e Nova Friburgo, Rio de Janeiro*. PhD Thesis, Universidade Federal do Rio de Janeiro, Rio de Janeiro, 198 p.

Liégeois J.P. 1998. Preface: Some words on the post-collisional magmatismo. *Lithos*, **45**:XV-XVII.

Ludka I.P., Mendes J.C., Penha H.M., Belmonte S., Almeida T. 2006. Considerações geoquímicas e idade U-Pb do Granito Parati, sul do estado do Rio de Janeiro. *In*: Congresso Brasileiro de Geologia, 43., Aracaju. *Annals...*, p. 253.

Ludwig K.R. 2001. *SQUID 1.02:* A User's Manual. Berkeley, Berkeley Geochronology Center Special Publication.

Ludwig K.R. 2012. User's Manual for Isoplot 3.75. Berkeley, Berkeley Geochronology Center Special Publication, 75 p.

Machado N., Valladares C.S., Heilbron M., Valeriano C.M. 1996. U-Pb geochronology of the central Ribeira Belt (Brazil) and implications for the evolution of the Brazilian Orogeny. *Precambrian Research*, **79**(3-4):347-361. https://doi.org/10.1016/0301-9268(95)00103-4

Martins G.G., Mendes J.C., Schmitt R.S., Armstrong R., Valeriano C.M. 2016. 550–490 Ma pre-to post-collisional shoshonitic rocks in the Ribeira Belt (SE Brazil) and their tectonic significance. *Precambrian Research*, **286**:352-369. https://doi.org/10.1016/j.precamres.2016.10.010

Medeiros S.R., Wiedemann C.M., Vriend S. 2001. Evidence of mingling between contrasting magmas in a deep plutonic environment: the example of Várzea Alegre in the Panafrican/Brasiliano Mobile Belt in Brazil. *Anais da Academia Brasileira de Ciências*, **73**(1):99-119. http://dx.doi.org/10.1590/S0001-37652001000100009

Medeiros S.R., Wiedemann-Leonardos C., Mendes J.C. 2000. Post-collisional multistage magmatism in the Ribeira Mobile Belt: geochemical and isotopic study of the Varzea Alegre Intrusive Complex, Espirito Santo, Brazil. *Revista Brasileira de Geociências*, **30**(1):30-34.

Mendes J.C., Junho M.B., Ghizi A. 2002. Geology and Geochemistry of granitic and dioritic rocks of the São José do Ribeirão intrusive massif, mountain region of Rio de Janeiro State, Brazil. *Revista UFRRJ*, Série Ciências Exatas e da Terra, **21**(2):1-11.

Mendes J.C., McReath I., Wiedemann C.M., Figueiredo M.C.H. 1997. Charnoquitóides do maciço de Várzea Alegre: um exemplo de magmatismo cálcio-alcalino de alto K no arco magmático do Espírito Santo. *Revista Brasileira de Geociências*, **27**(1):13-24.

Mendes J.C., Medeiros S.R., Chaves E.A. 2011. Assinatura isotópica de Sr e Nd do magmatismo cálcio-alcalino de alto-K na Faixa Ribeira central: o exemplo do Granito São Pedro em Lumiar. RJ. *Revista Brasileira de Geociências*, **41**(3):408-419.

Mendes J.C., Medeiros S.R., McReath I., De Campos C.M.P. 2005. Cambro-Ordovician magmatism in SE Brazil: U-Pb and Rb-Sr ages, combined with Srand Nd isotopic data of charnockitic rocks from the Varzea Alegre complex. *Gondwana Research*, **8**(3):337-345.

Middlemost E.A.K. 1989. Iron oxidation ratios, norms and the classification of volcanic rocks. *Chemical Geology*, **77**(1):19-26. https://doi.org/10.1016/0009-2541(89)90011-9

Milani E.J., Melo J.H.G., Souza P.A., Fernandes L.A., França A.B. 2007. Bacia do Paraná. *Cartas Estratigráficas: Boletim de Geociências da Petrobras*, Rio de Janeiro, **15**(2):265-287.

Moraes J.M. 2009. *Geologia do Granito Silva Jardim (RJ): Implicações na evolução tectônica dos Terrenos Oriental e Cabo Frio*. Thesis, Universidade Estadual do Rio de Janeiro, Rio de Janeiro, 65 p.

Morrison G.W. 1980. Characteristics and tectonic setting of the shoshonite rock association. *Lithos*, **13**(1):97-108. https://doi.org/10.1016/0024-4937(80)90067-5

Neto C.C.A., Valeriano C.M., Passarelli C.R., Heilbron M., Lobato M. 2014. Monazite ID-TIMS U-Pb geochronology in the LAGIR laboratory, Rio de Janeiro State University: protocols and first applications to the assembly of Gondwana supercontinent in SE-Brazil. *Anais da Academia Brasileira de Ciências*, **86**(1):171-186. http://dx.doi.org/10.1590/0001-3765201420120005

Osbourn E.F. 1959. Role of oxygen pressure in the crystallization and differentiation of basaltic magma. *American Journal of Science*, **257**(9):609-647. http://dx.doi.org/10.2475/ajs.257.9.609

Pacheco B.T. 2010. *Caracterização petrográfica e geoquímica das rochas do Corpo de Conselheiro Paulino (Suíte Nova Friburgo) na Região Serrana do Estado do Rio de Janeiro, RJ.* Monography, Universidade Estadual do Rio de Janeiro, Rio de Janeiro, 51 p.

Pearce J.A. 1996. Sources and settings of granitic rocks. *Episodes*, **19**(4):120-125.

Pearce J.A., Harris N.B.W., Tindle A.J. 1984. Trace element discrimination diagrams for the tectonic interpretation of granitic rocks. *Journal of Petrology*, **25**:956-983. http://dx.doi.org/10.1093/petrology/25.4.956

Peccerillo A., Taylor S.R. 1976. Geochemistry of Eocene calc–alkaline volcanic rocks from the Kastamonu area, Northern Turkey. *Contributions to Mineralogy and Petrology*, **58**(1):63-81. https://doi.org/10.1007/BF00384745

Pedrosa-Soares A.C., Alkmim F.F., Tack L., Noce C.M., Babinski M., Silva L.C., Martins-Neto M.A. 2008. Similarities and Differences between the Brazilian and African Counterparts of the Neoproterozoic Araçuaí-west Congo Orogen. *Geological Society Special Publications*, **294**:153-172. https://doi.org/10.1144/SP294.9

Platzer S. 1997. *Whole-rock geochemistry of the Araçê/Pedra Azul pluton*. Thesis, University of Utrecht, Netherlands, 58 p.

Potratz G.L., Valeriano C.M. 2017. Petrografia e Litogeoquímica do Granito Itaoca, Município de Campos dos Goytacazes, RJ: O Representante Mais Jovem do Magmatismo Pós-Colisional da Faixa Ribeira. *Geonomos*, **25**(1):1-13. https://doi.org/10.18285/geonomos.v25i1.908

Ribeiro R. 2006. *Estudo geológico e geoquímico preliminar do granito Silva Jardim, Rio de Janeiro*. Monography, Departamento de Geologia, Universidade Federal do Rio de Janeiro, Rio de Janeiro, 45 p.

Sato K., Tassinari C.C.G., Basei M.A.S., Siga Júnior O., Onoe A.T., Souza M.D. 2014. Sensitive high resolution ion microprobe (SHRIMP IIe/MC) of the Institute of Geosciences of the University of São Paulo, Brazil: analytical method and first results. *Geologia USP, Série Científica*, **14**(3):3-18. https://doi.org/10.5327/Z1519-874X201400030001

Sato K., Tassinari C.C.G., Kawashita K., Petronilho L. 1995. O Método Geocronológico Sm-Nd no IGc/USP e suas Aplicações. *Anais da Academia Brasileira de Ciências*, **67**(3):313-336.

Schmitt R.S., Trouw R., Van Schmus W.R., Armstrong R., Stanton N.S.G. 2016. The tectonic significance of the Cabo Frio Tectonic Domain in the SE Brazilian margin: a Paleoproterozoic through Cretaceous saga of a reworked continental margin. *Brazilian Journal of Geology*, **46**(Suppl. 1):37-66. http://dx.doi.org/10.1590/2317-4889201620150025

Schmitt R.S., Trouw R.A.J., Van Schmus W.R., Pimentel, M.M. 2004. Late amalgamation in the central part of Western Gondwana: new geochronological data and the characterization of a Cambrian collision orogeny in the Ribeira belt (SE Brazil). *Precambrian Research*, **133**(1):29-61. http://dx.doi.org/10.1016/j.precamres.2004.03.010

Shand S.J. 1943. *The Eruptive Rocks*. 2nd Ed. New York, John Wiley, 444 p.

Sial A.N., McReath I. 1984. *Petrologia Ígnea.* SBG, CNPq, Ed. Bureau, 180 p.

Söllner F., Lammerer B., Weber-Diefenbach K., Hansen B.T. 1987. The Brasiliano orogenesis, age determinations (Rb-Sr and U-Pb) in the coastal mountain region of Espírito Santo, Brazil. *Zentralblatt für Geologie und Paläontologie*, **7-8**:729-741.

Söllner F., Lammerer B., Wiedemann C.M. 2000. Dating the Ribeira Mobile Belt of Brazil. *Zeitschrift für Angewandte Geologie*, 245-255.

Stacey J.S., Kramers J.D. 1975. Approximation of terrestrial lead isotope evolution by a two-stage model. *Earth and Planetary Science Letters*, **26**(2):207-221. https://doi.org/10.1016/0012-821X(75)90088-6

Teixeira A.P.G. 2010. *Estudos geoquímicos comparativos de granitos tardi a pós-colisionais no segmento central do Orógeno Ribeira no Estado do Rio de Janeiro*. Monography, Universidade Federal do Rio de Janeiro, Rio de Janeiro, 45 p.

Trouw R.A.J., Heilbron M., Ribeiro A., Paciullo F., Valeriano C., Almeida J.C.H., Tupinambá M., Andreis R.R. 2000. The central segment of the Ribeira belt. In: Cordani U.G., Milani E.J., Thomaz–Filho A., Campos D.A. (eds.), *Proceedings of the 31st International Geological Congress*, Rio de Janeiro, Brazil, p. 287-310.

Trouw R.A.J., Peternel R., Ribeiro A., Heilbron M., Vinagre R., Duffles P., Trouw C.C., Fontainha M., Kussama H.H. 2013. A new interpretation for the interference zone between the southern Brasília Belt and the central Ribeira Belt, SE Brazil. *South American Earth Sciences*, **48**:43-57. http://dx.doi.org/10.1016/j.jsames.2013.07.012

Tupinambá M., Heilbron M., Duarte B.P., Nogueira J.R., Valladares C.S., Almeida J., Silva L.G. do E., Medeiros S.R. de, Almeida C.G. de, Miranda A., Ragatky C.D., Mendes J.C, Ludka I. 2007. Geologia da Faixa Ribeira Setentrional: estado da arte e conexões com a Faixa Araçuaí. *Geonomos*, **15**(1):67-79. https://doi.org/10.18285/geonomos.v15i1.108

Tupinambá M., Heilbron M., Valeriano C., Porto Jr. R., Dios F.B. Machado N., Silva L.G.E., Almeida J.C.H. 2012. Juvenile contribution of the Neoproterozoic Rio Negro Magmatic Arc (Ribeira Belt, Brazil): implications for Western Gondwana amalgamation. *Gondwana Research*, **21**(2-3):422-438. http://dx.doi.org/10.1016/j.gr.2011.05.012

Tupinambá M., Teixeira W., Heilbron M. 2000. Neoproterozoic Western Gondwana assembly and subduction-related plutonism: the role of the Rio Negro Complex in the Ribeira belt, South-eastern Brazil. *Revista Brasileira de Geociências*, **30**(1):7-11.

Valeriano C.M. 2012. *Geologia e Recursos Minerais da Folha Baía de Guanabara, SF-23-ZB-IV, escala 1:100.000, Nota Explicativa*. Programa Geologia do Brasil. Belo Horizonte, CPRM, 156 p.

Valeriano C.M., Mendes J.C., Tupinambá M., Bongiolo E.M., Aguiar Neto C.C., Silva L.G.E. 2017. *Magmatismo pós-colisional Neoproterozoico a Ordoviciano*. Geologia e Recursos Minerais do Estado do Rio de Janeiro: texto explicativo dos Mapas Geológico e de Recursos Minerais do Estado do Rio de Janeiro. Rio de Janeiro, CPRM.

Valeriano C.M., Mendes J.C., Tupinambá M., Bongiolo E.M., Heilbron M.C.P.L., Junho M.C.B. 2016. Cambro-Ordovician post-collisional granites of the Ribeira Belt, SE-Brazil: a case of terminal magmatism of a hot orogen. *Journal of South American Earth Sciences*, **68**:269-281. http://dx.doi.org/10.1016/j.jsames.2015.12.014

Valeriano C.M., Tupinambá M., Simonetti A., Heilbron M., Almeida J., Eirado Silva L. 2011. U-Pb LA-MC-ICPMS geochronology of Cambro-Ordovician post-collisional granites of the Ribeira Belt, southeast Brazil: Terminal Brasiliano magmatism in central Gondwana supercontinent. *Journal of South American Earth Sciences*, **32**(4):416-428. http://dx.doi.org/10.1016/j.jsames.2011.03.003

Verma S.K., Pandarinath K., Verma S.P. 2012. Statistical evaluation of tectonomagmatic discrimination diagrams for granitic rocks and proposal of new discriminant-function-based multi-dimensional diagrams for acid rocks. *International Geology Review*, **54**(3):325-347. http://dx.doi.org/10.1080/00206814.2010.543784

Verma S.P. 2005. *Estadística básica para el manejo de datos experimentales: aplicación en la Geoquímica (Geoquimiometría)*. México, Universidad Nacional Autónoma de México, 186 p.

Verma S.P., Cruz-Huicochea R., Díaz-González L., Verma S.K. 2015. A new computer program TecDIA for multidimensional tectonic discrimination of intermediate and acid magmas and its application to the Bohemian Massif, Czech Republic. *Journal of Geosciences*, **60**(4):203-218. http://dx.doi.org/10.3190/jgeosci.201

Verma S.P., Pandarinath K., Verma S.K., Agrawal S. 2013. Fifteen new discriminant-function-based multi-dimensional robust diagrams for acid rocks and their application to Precambrian rocks. *Lithos*, **168-169**:113-123. http://dx.doi.org/10.1016/j.lithos.2013.01.014

Verma S.P., Rivera-Gómez M.A. 2013. Computer programs for the classification and nomenclature of igneous rocks. *Episodes*, **36**(2):115-124.

Verma S.P., Verma S.K. 2013. First 15 probability-based multi-dimensional discrimination diagrams for intermediate magmas and their robustness against postemplacement compositional changes and petrogenetic processes. *Turkish Journal of Earth Sciences*, **22**:931-995. http://dx.doi.org/10.3906/yer-1204-6

Vernon R.H., Johnson S.E., Melis E.A. 2004. Emplacement-related microstructures in the margin of a deformed tonalite pluton: The San José pluton, Baja Califórnia, México. *Journal of Structural Geology*, **26**(10):1867-1884. https://doi.org/10.1016/j.jsg.2004.02.007

Voll G. 1976. Recrystallization of quartz, biotite and feldspars from Erstfeld to the Leventina Nappe, Swiss Alps, and its geological significance. *Schweizerische Mineralogische und Petrographische Mitteilungen*, **56**:641-647. http://doi.org/10.5169/seals-43709

Weaver B.L., Tarney J. 1984. Empirical approach to estimating the composition of the continental crust. *Nature*, **310**:575-577.

Wiedemann C.M., Penha H.M, Schmidt-Thomé R. 1987. Granitoids do Espírito Santo and Rio de Janeiro State. *Revista Brasileira de Geociências*, **17**(4):674-689.

Wilson M. 1989. *Igneous Petrogenesis*. London, Unwin Hyman Ltd., 466 p.